AES 8405461Q-3
Final Report

EVALUATION OF THE INTEGRITY OF EMBED SYSTEMS AT THE SOUTH TEXAS ELECTRIC GENERATING STATION

Prepared by

Erwin L. Capener
Russell C. Cipolla
Geoffrey R. Egan
Thomas J. Feiereisen
Steve R. Paterson

Aptech Engineering Services, Inc.
795 San Antonio Road
Palo Alto, California 94303

Prepared for

Bechtel Energy Corporation
5400 Westheimer Court
Houston, Texas 77252-2166
Attention: Mr. Nick Joonejo

January 1985

VERIFICATION RECORD SHEET

REPORT NO: AES 8405461Q-3

TITLE: Evaluation of the Integrity of Embed Systems at the South Texas Electric Generating Station

DATE: January 17, 1985

Originated by: _____ 1-17-85
Geoffrey R. Egan, Project Manager — Date

Checked and Verified by: _____ 1/17/85
Jeffrey L. Grover, Verifier — Date

Quality Assurance Review by: _____ 1/17/85
Jeffrey L. Grover, QA Engineer — Date

Quality Assurance by: _____ 1/17/85
Jeffrey D. Byron, QA Manager — Date

TABLE OF CONTENTS

ABSTRACT

This is a report on the structural integrity of embedded assemblies determined from an evaluation program performed by Aptech Engineering Services, Inc., (APTECH) for Bechtel Energy Corporation.

The embedded assemblies in question were field-fabricated at the South Texas Project and consist of ASTM A36 plates with welded anchor rods specified to be A36 material. During fabrication, some rods of ASTM A193-B7 material may have been inadvertently welded to the A36 plates using welding procedures intended for A36 materials. The work described herein was performed to determine the available load capacity of these potentially non-conforming weldments.

The load capacity program was based on tests of A193-B7 welded rod specimens prepared to simulate and/or bound the production field welding. Specific weld parameters were selected to conservatively represent metallurgical conditions that are consistent with the field welding characteristics.

Tensile tests were performed on specimens of three rod diameters with proportionate weld sizes. All tests were performed under the supervision of APTECH and Bechtel Materials and Quality Services (M&QS) Department.

In addition to the tensile tests, detailed metallurgical and fractographic examinations were performed to identify the material conditions resulting from these welds. As expected, hard heat affected zone regions were generated in the rod material and, in some cases, cracks attributed to the welding were observed.

The results of the tensile tests indicated that the available load capacity of the A193 rod weldments is adequate to develop the required design load dictated by the originally specified A36 rod material of one inch, one and one-half inch, and two inch diameters. The tested ultimate loads of such weldments were found (1) to afford adequate factors of safety with respect to the specified allowable loads for A36 rod weldments, and (2) to be equal or higher than the specified minimum ultimate strength of the A36 rods.

Examination of broken specimens indicated that the failure was controlled by the weld joint itself and not the properties of the heat treated A193 rod. Furthermore, fracture mechanics analysis confirmed that there was no potential for low stress brittle fracture, and that limit load analysis was the appropriate basis for the failure prediction model for the welded configurations under consideration.

In view of (1) the excellent load performance of the weldments, (2) the fact that low stress brittle fracture is not developed, and (3) the original design margins are retained, it is recommended that the embedded plates with welded rods of potentially A193 material be accepted "use-as-is".

Section 1
INTRODUCTION

BACKGROUND

Based on a previous separate investigation, it was determined that past procedures used in the South Texas Project (STP) for handling round rod stock material for the field fabrication of embedded plates with welded anchor rods could have led to comingling of ASTM A36 and A193 Grade B7 rod materials. The embedded plates are used in various buildings, of both Units 1 and 2 of the STP, including the reactor containment building (RCB), and the mechanical electrical auxiliary building (MEAB). The welded rods range in diameter from three quarter inch to two inches. The welding procedures used to fabricate these embedments were based on welding of A36 to A36 material, and accordingly, the inadvertent use of the procedures for welding comingled A193 rods to A36 plates was recognized to be a potential concern. Separate studies performed earlier indicated that the actual extent and the projected probability of the material comingling were acceptably low. Nevertheless, it was considered desirable to determine the structural reliability of the embedded plates by verifying the load capacity and fracture safety of plate assemblies postulated to have weldments of A193 rods to A36 plate.

The A193-B7 material, because of its higher carbon and alloy contents, is more hardenable than A36 material, and consequently, hard, heat affected zones (HAZ) could be expected to develop in the A193-B7-to-A36 weldments. The higher hardness potentially developed in the HAZ may also favor the formation of cracks as the weldment cools. These two effects, hard HAZs and the likelihood of the presence of cracks, may contribute to a degraded strength condition in the A193-B7 weldments.

Because of the concern for the degraded weld condition, Bechtel Energy Corporation and Aptech Engineering Services, Inc., developed an integrity evaluation program, which is the subject of this report.

INTEGRITY EVALUATION PROGRAM

Since hard HAZs will occur in the A193-B7-to-A36 weldments, a testing program was developed to determine the available load capacity of these weldments. The available load capacity can then be compared to the required design capacity to establish whether or not the factors of safety prescribed by the design criteria are satisfied.

To develop such a program, it is necessary to consider the important parameters that will affect the strength of the weldments made with the A193-B7 material. It is also important to consider the field welding conditions and what influence they might have on the load capacity of such weldments. In addition, the tests have to be performed in a controlled manner so that the results can be applied to the field condition. Finally, if cracks may be present in these details, the potential for brittle fracture must be evaluated to establish whether or not brittle fracture is likely in the field condition.

All of these aspects have been considered in the work described herein. The metallurgy of the affected weldments has been established, and the test specimens used to determine load capacity have been designed to conservatively represent field welding conditions. Strength and fracture mechanics analyses have also been performed to confirm the test results.

OBJECTIVES

The objectives of the proposed work are as follows:

- To establish the metallurgical characteristics of the welds that potentially have been used to join the A193 rods to the A36 embedded

plates. This information is essential to be able to define designs for test specimens that represent the field condition. It is also necessary to determine the importance of the various welding parameters within the constraints of the field welding procedures.

- To develop series of test specimens that bound the field conditions in terms of bolt material, size, and welding process. These test series, representative of field conditions, can then be used to establish a measure of the load capacity for the A193-B7/A36 weldments.

- To perform load tests to establish a statistical measure of the welded rod load capacity for the test series identified. The data resulting from these tests may be used to define an available load capacity. This available load capacity can be established on a number of bases, including bounding statistics.

- To compare the test results with the required load capacity for the design case. This will give an assessment of the consequences of the A193-B7 weldments on the structural integrity of the embedded plates.

Section 2
SCOPE

To achieve the above objectives, a program consisting of the following four tasks was identified:

Task 1 - Design of Test Program to be a Conservative Representation of Field Conditions

Task 2 - Monitoring of Tests

Task 3 - Analysis of Results and Evaluation of the Significance of the Results

Task 4 - Conclusions and Recommendations

The following sections of the report detail the results of the tests and analyses.

In Section 3, the basis for the test specimen matrix is developed taking into account the field welding conditions and their influence on the test data. The variables to be used in the production of the test specimens and the tests to determine load capacity values are established.

In Section 4, the results of the tests are described, including the metallurgical studies performed by Bechtel (M&QS) and APTECH. In Section 5, the significance of the results is outlined in a comparison of tested load capacity with required design capacities. The conclusions and recommendations are outlined in Section 6.

Section 3
TEST MATRIX DESIGN

INTRODUCTION

To establish the available load capacity, a series of test specimens were developed to provide load capacity data for the weldment between A193 rod and A36 plate. To meet the objectives of this program, the tests were designed to include all of the effects of field welding and to bound the metallurgical conditions that could result in these welds.

The objectives of the test plan were as follows:

- Determine the number of specimens to be tested to establish a measure of load capacity
- Provide details of weld procedures to prepare specimens which conservatively represent the field welding conditions
- Provide details of the test, including test specimen and fixture design and instrumentation
- Provide a format for performing the tests and recording the results

WELDING PARAMETERS

There are two conditions that may exist when low alloy quenched and tempered (LAQT) rods of A193-B7 material are welded to A36 plates using welding procedures intended for A36 material. First, because of the high hardenability of A193 material, a hard HAZ may be formed. The formation of hard HAZs is controlled by cooling rate (as affected by arc energy or heat input from the welding arc, preheat, material size, interpass termperature,

and material chemical composition) as it affects the potential to form hard regions with heat treatment (hardenability). Second, in cases where excess heat may be used during the welding process, it could be postulated that overtempering could lead to a softening of the subcritical HAZ and a resultant loss of strength. The weldability tests described herein were designed to simulate these two extreme welding conditions. A detailed description of each of these conditions follows.

HEAT AFFECTED ZONE HARDENING

The propensity for a material to form a hard microstructure can be estimated from a hardenability index expressed as a carbon equivalent (CE). This is an empirically derived relationship that takes into account those chemical constituents of the metal that promote hardening when heat treated. The CE is based on steel composition. A frequently used formula for CE is:

$$CE = C + Mn/6 + (Cr + Mo + V)/5 + (Ni + Cu)/15 \qquad (3\text{-}1)$$

If the chemistry tolerances of A36 are met, then the maximum CE level (assuming a weight % Cu = 0.2) obtainable for this material is 0.46. In comparison, A193-B7 material may have CE levels ranging from 0.66 to 0.96, indicating a significantly higher hardenability than A36 material (Table 3-1). This means that special precautions (such as preheat, high arc energy, post-weld heat treatment, etc.) would normally be considered when welding these materials to avoid hard HAZs susceptible to cracking. Since these precautions were not taken (the potentially comingled A193-B7 rods were welded with a welding procedure intended for A36 materials), the test specimen weld procedures should reflect the adverse welding conditions that will produce such HAZs.

For the case of the A193-B7 rods, the adverse field welding will occur when:

- The rod is the largest size permitted by the design. For a fixed arc energy, the largest rod will give the greatest heat sink and,

Table 3-1

CHEMISTRY TOLERANCES OF A36 AND A193-B7 (WT %)

Element	A36 (3/4" - 1-1/2" Thick)	A193-B7
C	0.25 max	0.37 - 0.49
Mn	0.80 - 1.20	0.65 - 1.10
P	0.04 max	0.035 max
S	0.05 max	0.040 max
Si	---	0.15 - 0.35
Cu	0.20 min	---
Cr	---	0.75 - 1.20
Mo	---	0.15 - 0.25
Carbon Equivalent	0.46	0.66 - 0.96

hence, the highest cooling rate. This, in turn, gives the greatest propensity to form martensite on cooling, a transformation product with high hardness.

- The weld is the smallest. This promotes low arc energy, which again implies high cooling rates and high hardnesses.

- The minimum preheat value is used. The use of preheat provides slower cooling rates, and conversely, the minimum preheat will give the worst case cooling rate.

SUSCEPTIBILITY TO CRACKING

The adverse field welding conditions that may produce cracking were promoted by introducing conditions conducive to high hardness. The presence of hydrogen in the weld pool, which may also lead to cracking, was not deliberately introduced since normal field electrode control procedures that effectively preclude that cracking were used in the prior field welding of plates as well as in the preparation of the welded specimens.

The ways of controlling the volume of martensite (a hard susceptible microstructure) have been discussed previously. Again, the arc energy, preheat and postheat levels control the amount and type of transformation products formed.

TEST MATRIX

In view of the above considerations, the test matrix shown in Table 3-2 was developed to simulate the adverse welding conditions expected to produce degradation of an A193-B7 rod to A36 plate weldment when it is performed using the specified welding procedures. A nominal sample size of ten specimens for each of the three rod diameters was selected initially. The minimum rod size of one inch for the tests was selected based on the fact that the one inch rod with a 3/8 inch leg length fillet would harden more than the 3/4 inch rod with a 5/16 inch leg length fillet.

Table 3-2

TEST MATRIX AND WELDING PARAMETERS

Test Number	A1	A2	B	C	D
A193 Rod Dia	1"	1"	1"	1 1/2"	2"
Preheat	N/A	N/A	N/A	N/A	150°F
Interpass	N/A	N/A	N/A	50°F min.	150°F min.
Test Position	1F (Fillet)	1G (Full penetration)	1F (Fillet)	1F (Fillet)	1F (Fillet)
CE	0.777	0.777	0.795	0.817	>0.8
Rod Heat No./Code	8866608/ADV	8866608/ADV	93031/AVF	75973/AVM	8895931/AEA
Weld Size	5/8"	5/8"	3/8"	1/2"	5/8"
Bead Type	Root Pass/Stringer Capping Pass/Weave	Root Pass/Stringer Fill Passes/Weave Capping Pass/Weave	All Passes/ Stringer	All Passes/ Stringer	All Passes/ Stringer
A36 Plate Size	4"x4"x1 1/2"	4"x4"x1 1/2"	4"x4"x1 1/2"	4"x4"x1 1/2"	5 1/2"x5 1/2x1 1/2"
E7018 Electrode Size	3/32" Dia	3/32" Dia	3/32" Dia	3/32" Dia	3/32" Dia
Amperage	110-120	110-120	76-90	76-90	76-90
Arc Voltage	25-28	25-28	19-22	19-22	19-22
Travel Speed*	2.1-2.6 in/min	2.1-2.6 in/min	3.1-4.3 in/min	3.1-4.3 in/min	3.1-4.3 in/min
Heat Input (Max.)	70 KJ/in	70 KJ/in	25KJ/in	25 KJ/in	25 KJ/in
Number/Passes	>2	>2	2	>2	>2
Number/Tests	2	2	22	12	12

*Travel speed should be monitored during welding.

OVER TEMPERING

Test Series A, as defined in Table 3-2 prescribes the highest expected arc energy and smallest rod diameter used, thus, it provides a condition in which a maximum amount of subcritical HAZ tempering would occur. These specimens were used for metallurgical evaluation only since the annealed or fully tempered A193 would still be stronger than the A36 bolt material (1). Test Series B, C and D prescribe conditions whereby minimum arc energy and preheat values were used to weld the A193-B7 rods of diameters consistent with the diameters used on the STP embedded plates. These tests were set up to maximize the cooling rates of the weldments and, thus, maximize the potential metallurgical degradation of the welded joint. For each test series, two additional welded specimens were prepared for metallurgical evaluation so that the expected metallurgical conditions could be confirmed.

This test matrix and parameters permitted representation of the adverse welding conditions that could be associated with the STP welding of the A193-B7 rods to A36 plate. Thus, using these parameters, a lower bound for the available load capacity of the STP welded rods was obtained.

TEST METHOD AND PARAMETERS

In the service situation, a particular embedded plate may be used for different functions, such as beam end connections, pipe whip restraint supports, pipe hanger attachments, etc. Under all circumstances, the predominant loads on the embedded plate will result in axial load and shear on the welds. Accordingly, as a conservative approach, all tests were performed in axial tension. This loading is considered to be the most discriminating case as it subjects the entire weld area to tension, and any expected cracks at the weld toe or root would be expected to perform worse under this loading condition. The design of the specimen was such as to account for bearing stresses, plate thickness, and rod length for gripping.

The test specimen design shown in Figures 3-1 and 3-2 was used for all tests.

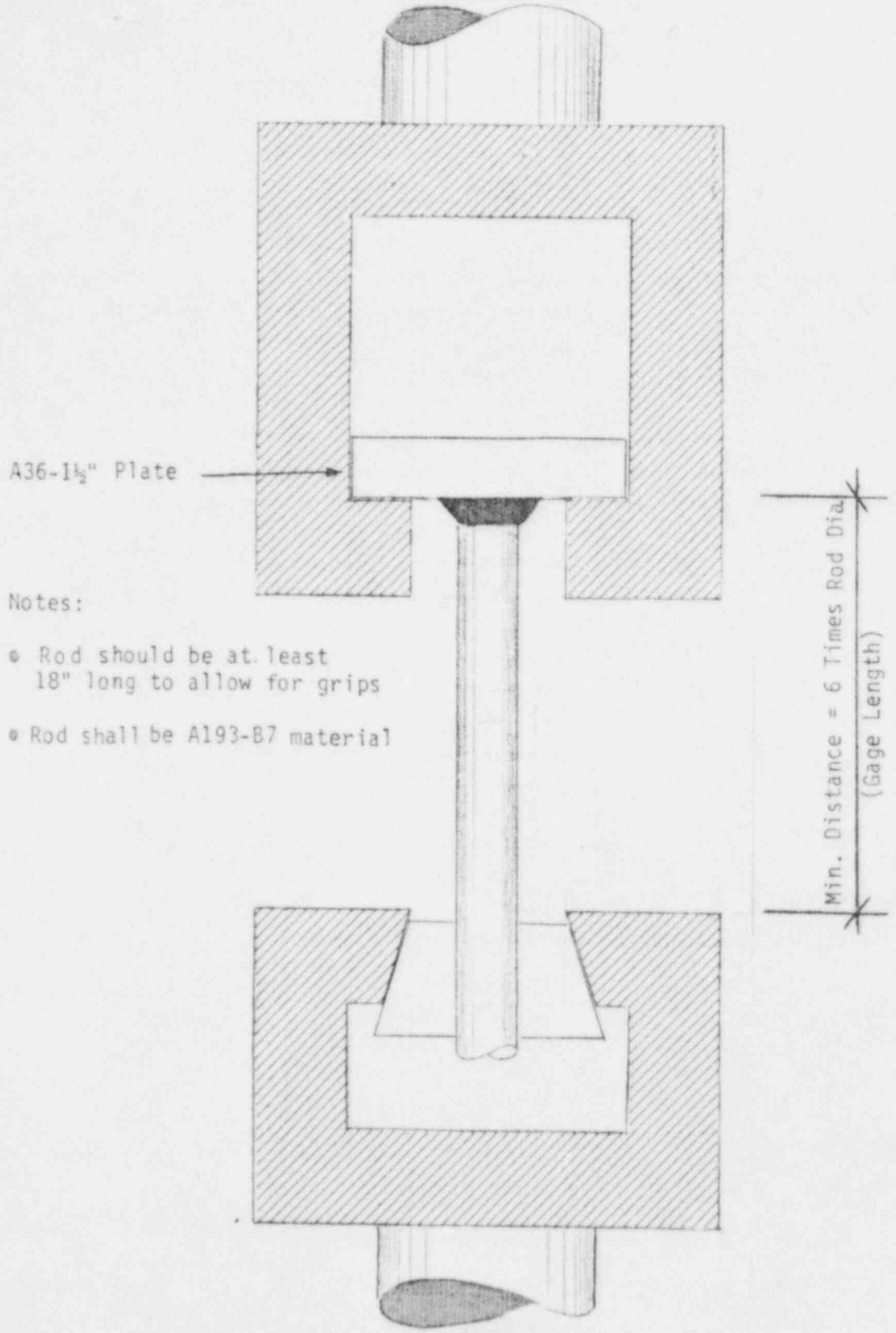

Figure 3-1 - Weld Test Apparatus and Specimen.

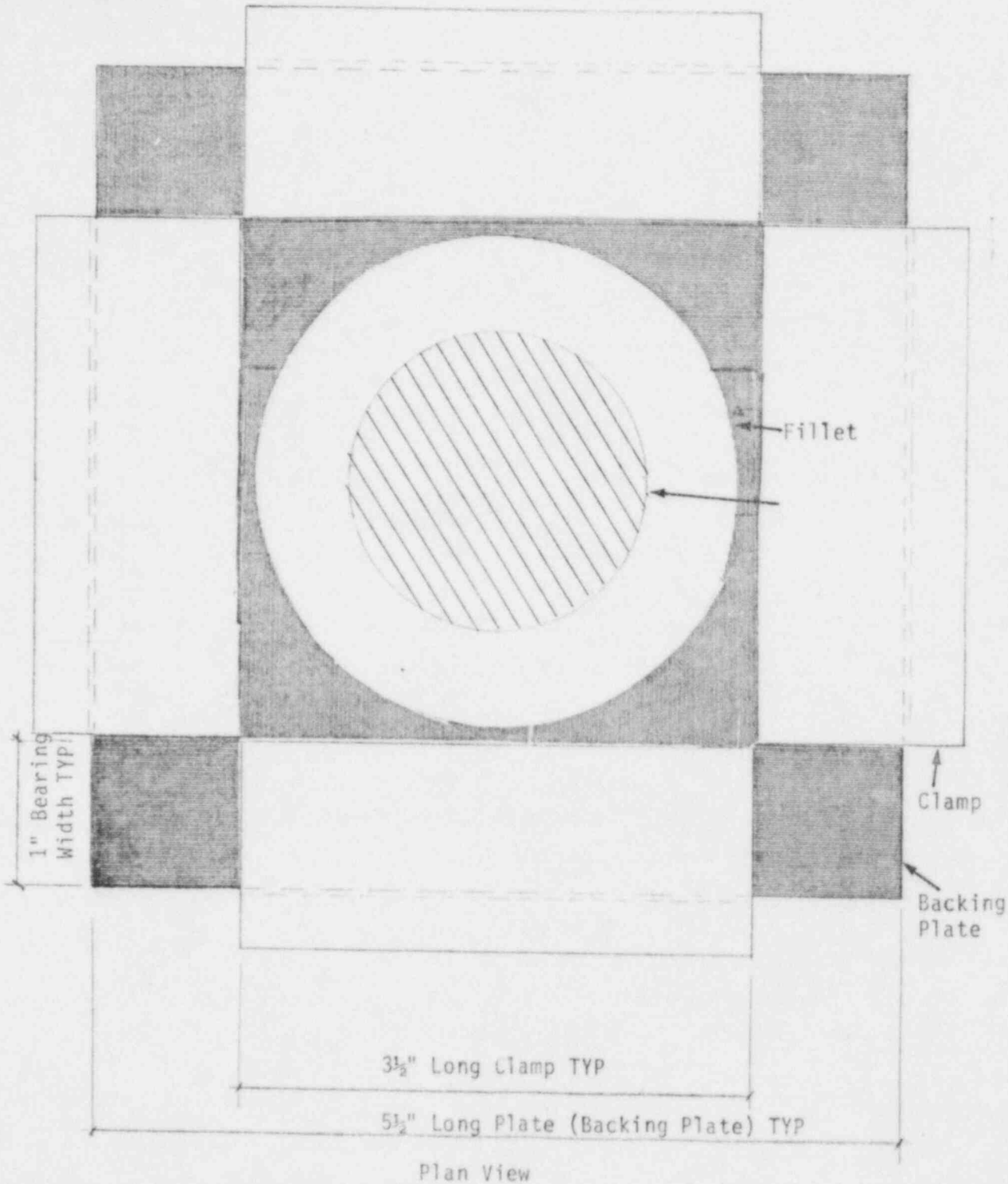

Figure 3-2 - Schematic of Backing For Tension Tests.

Section 4
TEST RESULTS

INTRODUCTION

The specimens for the test matrix identified in Table 3-2 were welded at the STP site using field welding conditions modified as defined in Table 3-2. All welding was done by Ebasco under Bechtel's direction. APTECH personnel also witnessed the production of some of these welds at the site. Upon completion, the specimens were shipped to Bechtel M&QS in San Francisco for visual and dye penetrant examinations. In addition, metallurgical examinations and fractographic studies were performed by APTECH and Bechtel M&QS.

The tensile tests were performed at three testing laboratories based on the capacity of the testing equipment. A typical test setup showing the dial indicators for displacement measurement is shown in Figure 4-1. Bechtel M&QS started the B-series testing and broke several specimens. The remaining B-series specimens exceeded their equipment capacity (60 KIPS) and were subsequently tested to failure at Anamet Laboratories. All C and D series specimens were broken on the 600 KIP machine at Pittsburg Testing Laboratories. Failure strengths, weld leg lengths, and crack dimensions, if any, are shown in Table 4-1 (2).

INSPECTION RESULTS

The visual inspection revealed that the welds for all test series (A, B, C, and D) were of acceptable quality, exhibiting some minor areas of undercut. Typical weld appearance is shown in Figure 4-2. Dye penetrant examination was performed to detect the presence of surface cracking. No surface cracking was observed.

(A)

(B)

Figure 4-1 - Details Of Test Set-up.

Table 4-1

TEST RESULTS FOR A193 B-7 ANCHOR ROD WELDED TO A36 PLATE

Specimen No.	Rod Size (In.)	Average Weld Length (In.)	Crack Depth (In.)	Crack Width (In.)	Weld Failure Strength (KIPS)
B1	1	0.44			55.7
B3	1	0.45	0.12	0.45	63.2
B4	1	0.49			68.8
B5	1	0.46			61.8
B6	1	0.44			55.4
B7	1	0.39			47.3
B9	1	0.44	0.2, 0.1	0.4, 0.35	65.0
B10	1	0.44	0.25	0.4	62.2
B13	1	0.47			59.8
B14	1	0.44			67.2
C1	1½	0.54	0.25, 0.2	1.9, 0.3	125.4
C2	1½	0.64	0.1, 0.2	0.2, 0.9	151.0
C3	1½	0.58*	0.2, 0.2, 0.2, 0.1	0.5, 1.1, 0.2, 0.2	135.0
C4	1½	0.62*	0.3, 0.2	0.8, 1.6	142.5
C5	1½	0.59			132.5
C6	1½	0.61			143.0
C8	1½	0.59			147.0
C9	1½	0.56	0.25	2.25	125.0
C10	1½	0.59	0.25	1.25	141.5
C12	1½	0.58	0.15, 0.25	0.8, 0.6	137.5
D1	2	0.73			240.5
D2	2	0.73			241.25
D3	2	0.72	0.2	0.4	222.5
D4	2	0.75	0.25, 0.25, 0.1	3.5, 0.3, 0.25	222.75
D5	2	0.74			247.25
D7	2	0.70			237.5
D8	2	0.72	0.1	0.6	226.25
D10	2	0.69			226.5
D11	2	0.75	0.1	0.3	255.0
D12	2	0.73			237.75

*APTECH measurements

Interoffice memorandum, G. R. Schmidt to R. W. Straiton, Anchor Bolt Evaluation, South Texas Project, Job 146926-001, GRS-094-03 (September 10, 1984).

Interoffice memorandum, G. R. Schmidt to R. W. Straiton, Anchor Bolt Evaluation, South Texas Project, Job 14926-001, GRS-074-13 (June 27, 1984).

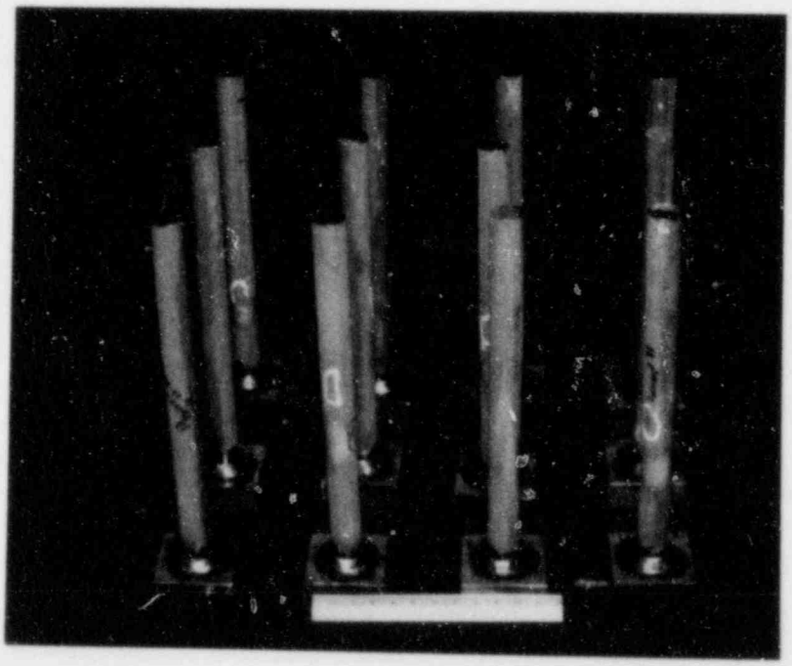

Figure 4-2 - Typical Appearance of Welded Test Specimens.

METALLURGICAL RESULTS

In the original test matrix, Series A1 and A2 specimens were welded for metallurgical examination only. These specimens were welded using high arc energy with a fillet (Series A1) and full penetration (Series A2) weld. The metallurgical examination was done to confirm that with these welding conditions (which produce slower cooling rates), the HAZ would not be as hard as for Series B, C, and D.

The specimens were sectioned on a diameter and polished and etched. Figure 4-3 is typical of the microstructure from these welds. For Series A2 (full penetration welds) the last pass of the weld was still exceptionally hard (~750 HV10) indicating that even for the high arc energy/slow cooling rate, hard HAZ regions are still formed (Figure 4-4).

Martensite typically is formed in such high hardness regions, and an example is shown in Figure 4-5.

Macro sections were also made from the two additional specimens from Series B, C, and D, and these are shown in Figures 4-6, 4-7, and 4-8, respectively. Regions of high hardness (martensite) are present, and in some cases, root cracks were present.

In conclusion, the effects of arc energy input and cooling rate do not significantly affect the hardness of the HAZ, and it is not essential to impose strict bounds on these parameters in order to obtain weld specimens adversely affected by hard HAZ.

HARDNESS RESULTS

Microhardness measurements were made for all test series welded, and the results are shown in Table 4-2 (2). The peak values of HAZ hardness are summarized in Table 4-3. There is no apparent HAZ hardness bias with respect to design cooling rate, which simply reflects the very high hardenability of the A193-B7 material. This means that the variations in welding parameters

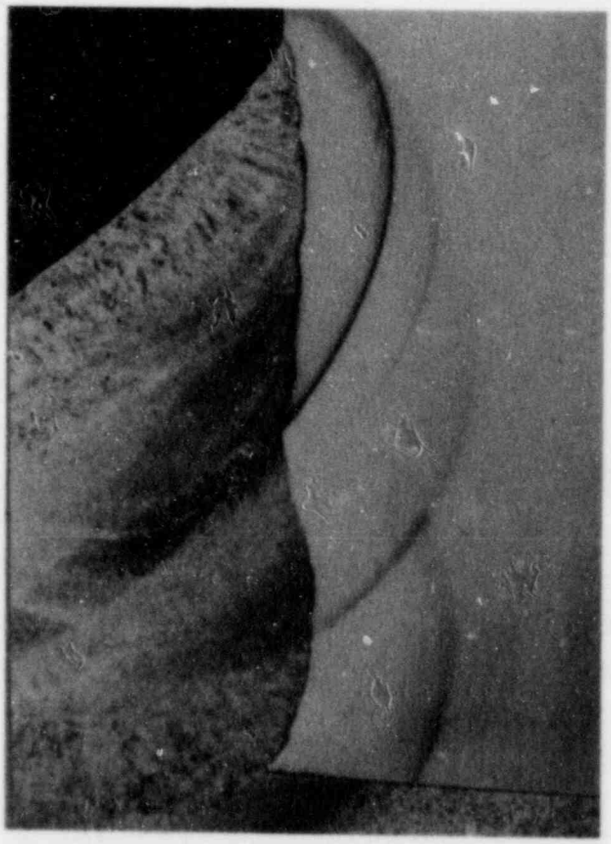

Figure 4-3 - Photomicrograph Typical of the Sections Made in Specimen A1-1.

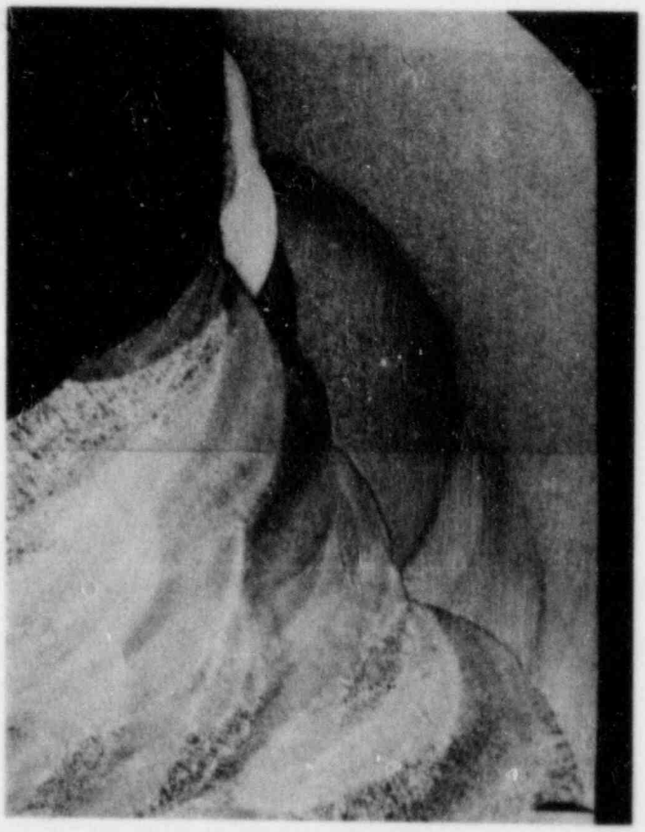

5X, Nital

Figure 4-4 - Weld Profile of Specimen A2-1 (Full Penetration Weld).

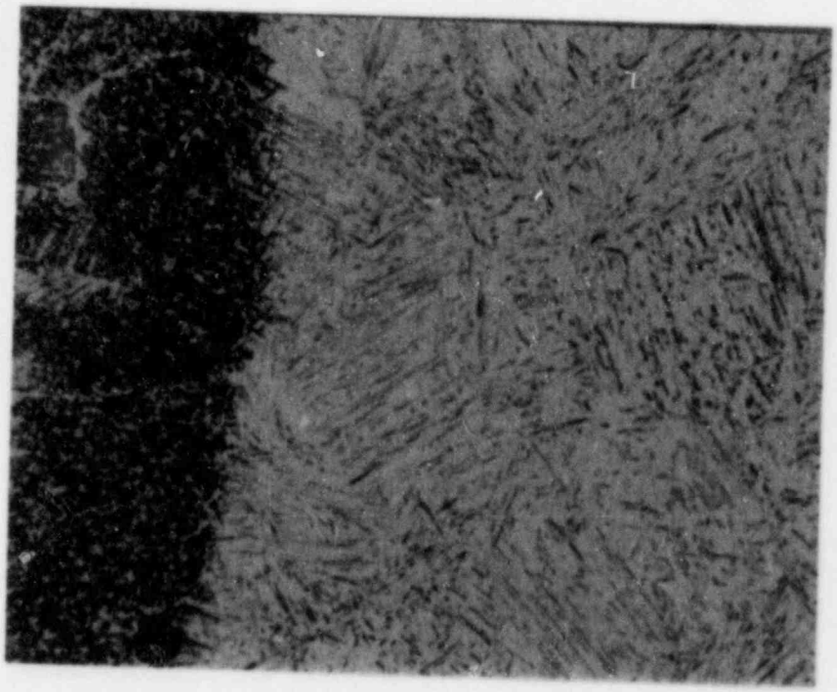

500X, Nital

Figure 4-5 - Photomicrograph of Detail of Figure 4-4. White Area to Right is Martensite.

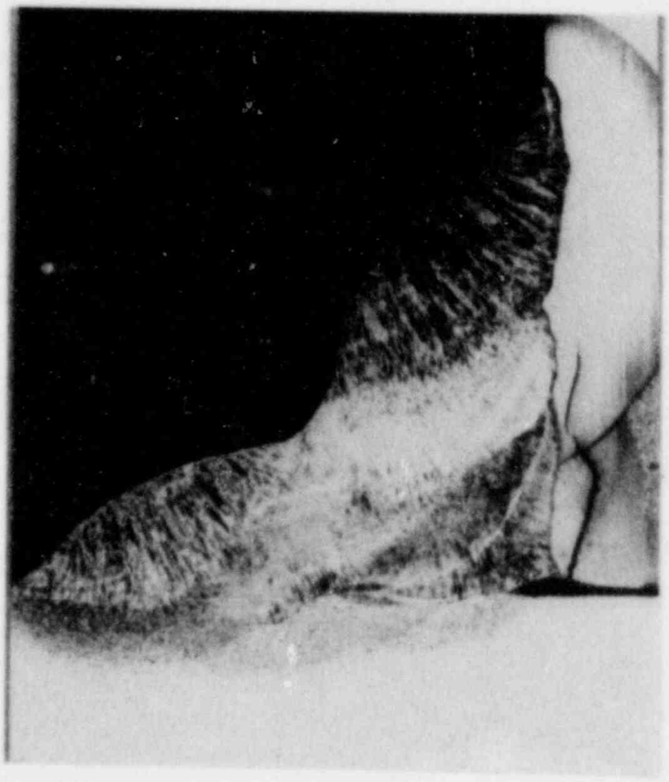

5X, Nital

Figure 4-6 - Weld Profile For Specimen B2.

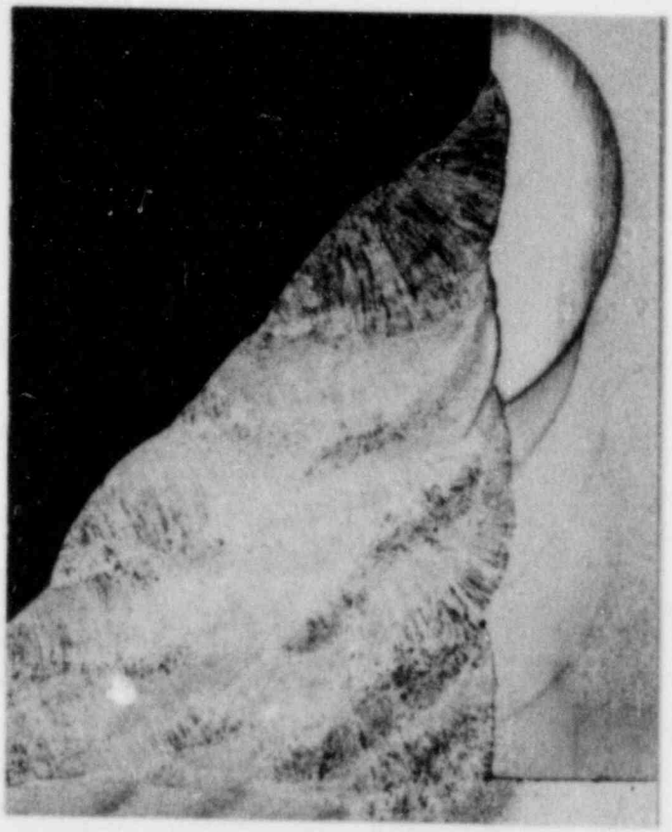

5X, Nital

Figure 4-7 - Photomacrograph of Specimen C11.

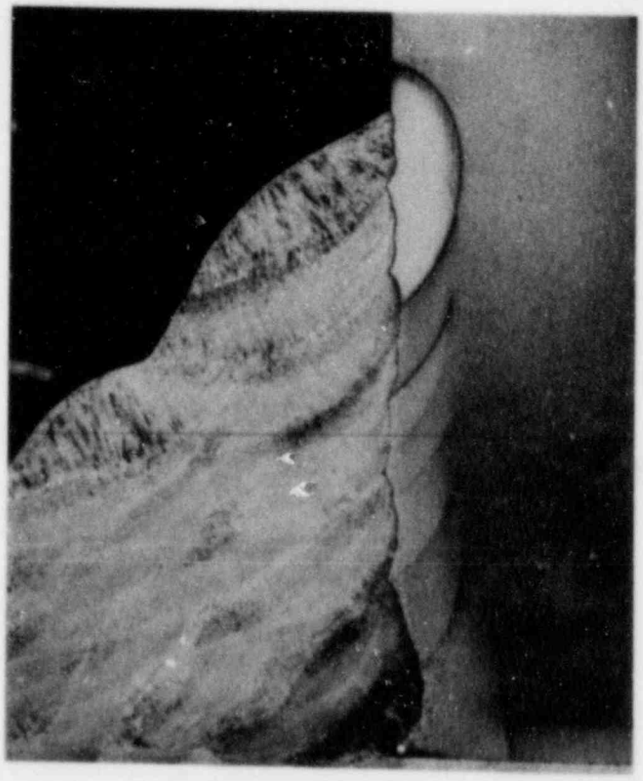

5X, Nital

Figure 4-8 - Photomacrograph of Specimen D9.

Table 4-2
MICROHARDNESS TEST RESULTS

Specimen Number	Bolt		Weld Metal	Plate	
	Base Metal	HAZ (Note 2)		HAZ (Note 3)	Base Metal
A1-1A	333	493, 461, 471	178, 193, 171	191, 189, 176	175
A1-1B	362	498, 566, 560	180, 165, 178	211, 202, 198	174
A1-2A	306	327, 409, 525	193, 177, 183	188, 181, -	157
A1-2B	362	528, 665, 631	198, 170, 178	189, 189, 183	170
A2-1A	289	473, 560, 579	185, 180, 175	181, 192, -	155
A2-1B	360	724, 752, 681	213, 189, 205	210, 211, 220	177
A2-2A	356	357, 370, 368	185, 177, 170	173, 179, 180	162
A2-2B	342	325, 336, 365	188, 167, 170	181, 178, 182	165
B2A	343	686, 646, 631	207, 200, 204	219, 238, 238	172
B2B	336	669, 743, 752	216, 225, 209	266, 252, 232	167
B8A	281	536, 478, 413	225, 210, 198	213, 218, -	171
B8B	351	642, 711, 703	220, 197, 213	250, 249, 210	162
C7A	319	408, 642, 639	190, 179, 221	210, 193, -	159
C7B	353	563, 649, 698, 703	189, 193, 211	227, 207, 181	172
C11A	332	694, 686, 653	200, 193, 197	203, 206, 192	172
C11B	350	686, 703, 677	192, 198, 198	217, 219, 195	160
D6A	297	566, 642, 599	266, 230, 216	279, 213, -	168
D6B	350	453, 466, 301	228, 216, 220	220, 219, 187	172
D9A	336	698, 653, 638	209, 197, 203	192, 194, 202	166
D9B	341	681, 711, 681	201, 199, 202	228, 222, -	167

NOTES: 1) See Table 4-4 for typical locations of hardness indentations.

2) Traverse from edge of base metal to near fusion line.

3) Traverse from near fusion line to edge of base metal HAZ.

Table 4-3

PEAK VALUES OF HEAT AFFECTED ZONE HARDNESS

Series	Rod Diameter (In.)	Description	Maximum Hardness (HV 10)
A1	1	High heat input, fillet weld	665
A2	1	High heat input, full penetration weld	752
B	1	Low heat input, fillet weld	752
C	1½	Low heat input	703
D	2	Low heat input and preheat	711

outlined in Table 3-2 have led to insignificant or indistinguishable differences in metallurgical condition. All of the resultant HAZs are very hard, irrespective of the variations introduced in the welding of the specimens.

In addition to the hardness values reported in Table 4-2, specific hardness traverses were performed in Specimens B8 and C7. These results are shown in Table 4-4 (3). It can be seen from these results that the hardest material resides in areas heated by the last weld bead and that regions near the root of the weld appear to have been tempered by successive weld passes.

ANALYSIS OF RESULTS

Weld Strengths

The tested failure loads plotted on logarithmic probability scales indicate a log normal distribution (Figure 4-9). The statistical properties of these welded specimens and estimates of the 90% confidence level, 95% probability population lower bounds are in Table 4-5.

The statistical interpretation of these lower population bounds is as follows. It is estimated at the 90% confidence level that 95% of the population of A193 rod to A36 plate weldments resulting wher the specified weld procedure is used with the given rod sizes will have load capacities of the stated value or greater. The data for the one inch diameter rod indicate at a 90% confidence, 95% probability level a lower bound load capacity that is slightly below the minimum specified ultimate load for a one inch diameter A36 rod (i.e., 90%/95% lower bound of 45.3 KIPS versus specified ultimate tensile load of 45.6 KIPS). For the one and one-half inch and two inch diameter rods, the 90%/95% lower bound load capacities of the A193 weldments exceed the specified ultimate loads for A36 rods of equivalent diameter. Therefore, embedded plates potentially containing A193 rods of these sizes will exceed the load capacity of the same plates containing A36 rods. APTECH considers the 90% confidence, 95% probability level as a conservative bound (Appendix A).

Table 4-4

HARDNESS TRAVERSES FOR SPECIMENS C7A AND B8B

C7A Location	Hardness HV10	Comments
1	228	Weld Metal
2	645	HAZ
3	329	HAZ
4	318	Base Metal
5	194	Weld Metal
6	360	HAZ
7	339	HAZ
8	294	Base Metal
9	210	Weld Metal
10	342	HAZ
11	380	HAZ
12	313	Base Metal
13	325	Base Metal

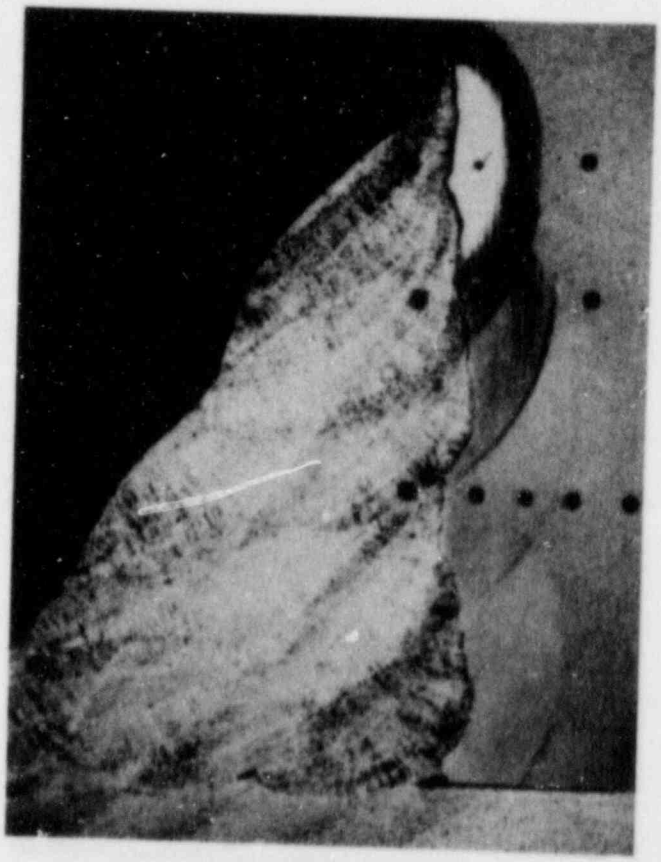

Hardness Locations

1 - 4

5 - 8

9 - 13

Bolt

Plate C7A, 5X, Nital

(TABLE 4-4 - Continued)

B8B Location	Hardness HV10	Comments
1	251	Weld Metal
2	715	HAZ
3	698	HAZ
4	505	HAZ
5	322	Base Metal
6	234	Weld Metal
7	715	HAZ
8	704	HAZ
9	525	HAZ
10	334	Base Metal
11	343	Base Metal
12	384	Weld Metal
13	411	HAZ
14	380	HAZ
15	343	Base Metal

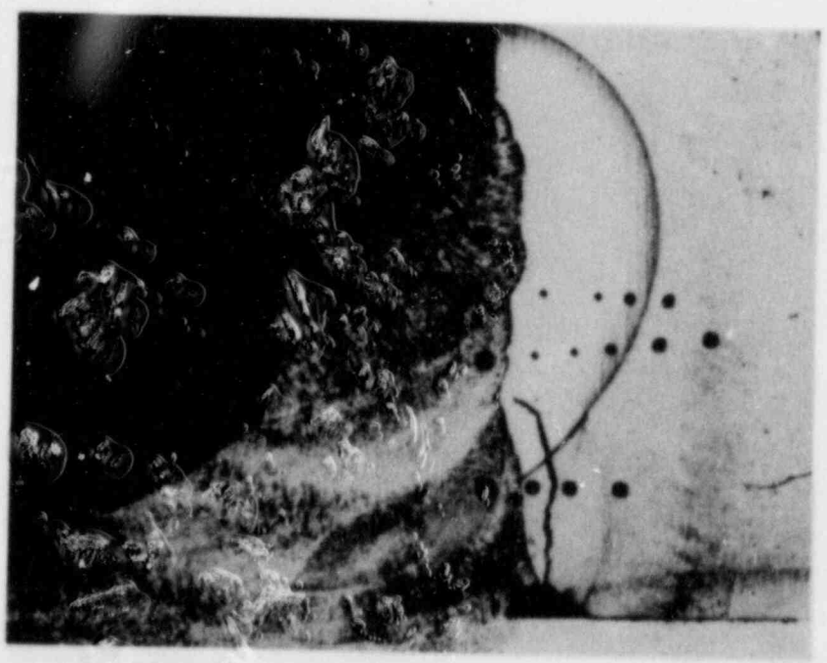

Bolt

Hardness Locations

1 - 5
6 - 11

12 - 15

Plate

B8B, 5X, Nital

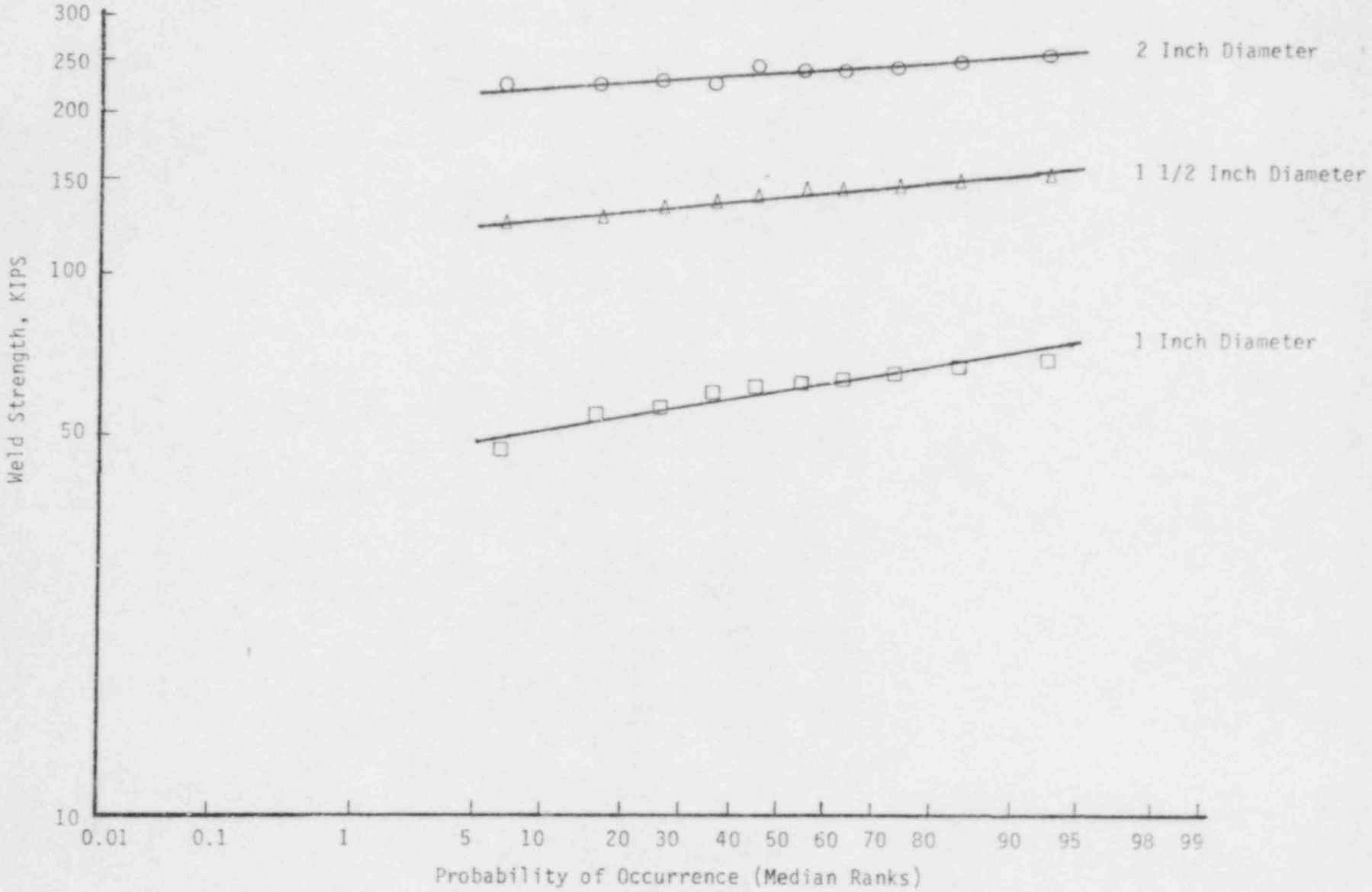

Figure 4-9 - Weld Strengths of A193 Anchor Rods Welded to A36 Plate.

Table 4-5

STATISTICAL PARAMETERS FOR SPECIMENS
AND REPRESENTATIVE POPULATIONS

	Rod Size, In.		
	1.0	1.5	2.0
Ln Mean (KIPS), $\bar{x}$	4.09959 (60.3)	4.92575 (137.8)	5.46170 (235.5)
Ln Standard Deviation, σ	0.11108	0.063335	0.046345
Number of Specimens, n	10	10	10
K Factor, One-Sided, 90%/95% (1)	2.568	2.568	2.568
Lower Population Bound, Ln (KIPS) (2)	3.81434 (45.3)	4.76311 (117.1)	5.34268 (209.1)
Specified Ultimate Tensile Load for A36 Rod, KIPS, Per Original Design	45.6	102.5	182.2

(1) "Factors for One-Sided Tolerance Limits and for Variables and Sampling Plans," Sandia Corporation, Monograph SCR-607 (March 1963).

(2) Lower Bound Limit = $\bar{x} - K\sigma$; Charles Lipson and Narenda Sheth, "Statistical Design and Analysis of Engineering Experiments," McGraw Hill Book Company, p. 79 (1973).

ANALYSIS OF DISPLACEMENT MEASUREMENTS

The testing system shown in Figure 4-1 or a modification thereof was used to test the welded rod specimens. The rods were gripped at a convenient distance from the weld (from 11 to 15 inches depending on rod size), and the displacement was measured with a dial indicator over this gauge length. In addition, on some of the B series tests a near-weld displacement measurement was made by placing a dial indicator to measure the displacement over a gauge length of approximately 0.65 inch, which encompased the weld.

All of the displacement data from the dial indicators measuring over the rod gauge length (2) were plotted against load, and a typical result from the 30 tests is shown in Figure 4-10.

These load displacement plots indicate that for all tests, the rod is experiencing elastic loading only and the controlling element for joint capacity is the weld.

In some cases, some nonlinearity was detected at the beginning of the test as the grips bedded into the bolt and as maximum load was approached. This latter non-linearity is attributed to the large displacements associated with weld pull out and failure.

To estimate the approximate strain developed within the weld joint region, the elastic displacement of the rod length (derived from the failure stress and Young's modulus) was calculated and subtracted from the total measured displacement accounting for the non-linearity. The resultant displacement remaining is that which takes place in the weld joint region. A weld joint pseudo strain can then be estimated by assuming a gauge length equal to the weld leg length. The displacements and resultant pseudo strains are summarized in Table 4-6. Typically, the tabulated values indicate that the weld joints are capable of undergoing considerable deformation, which is an indication of favorable ductile behavior.

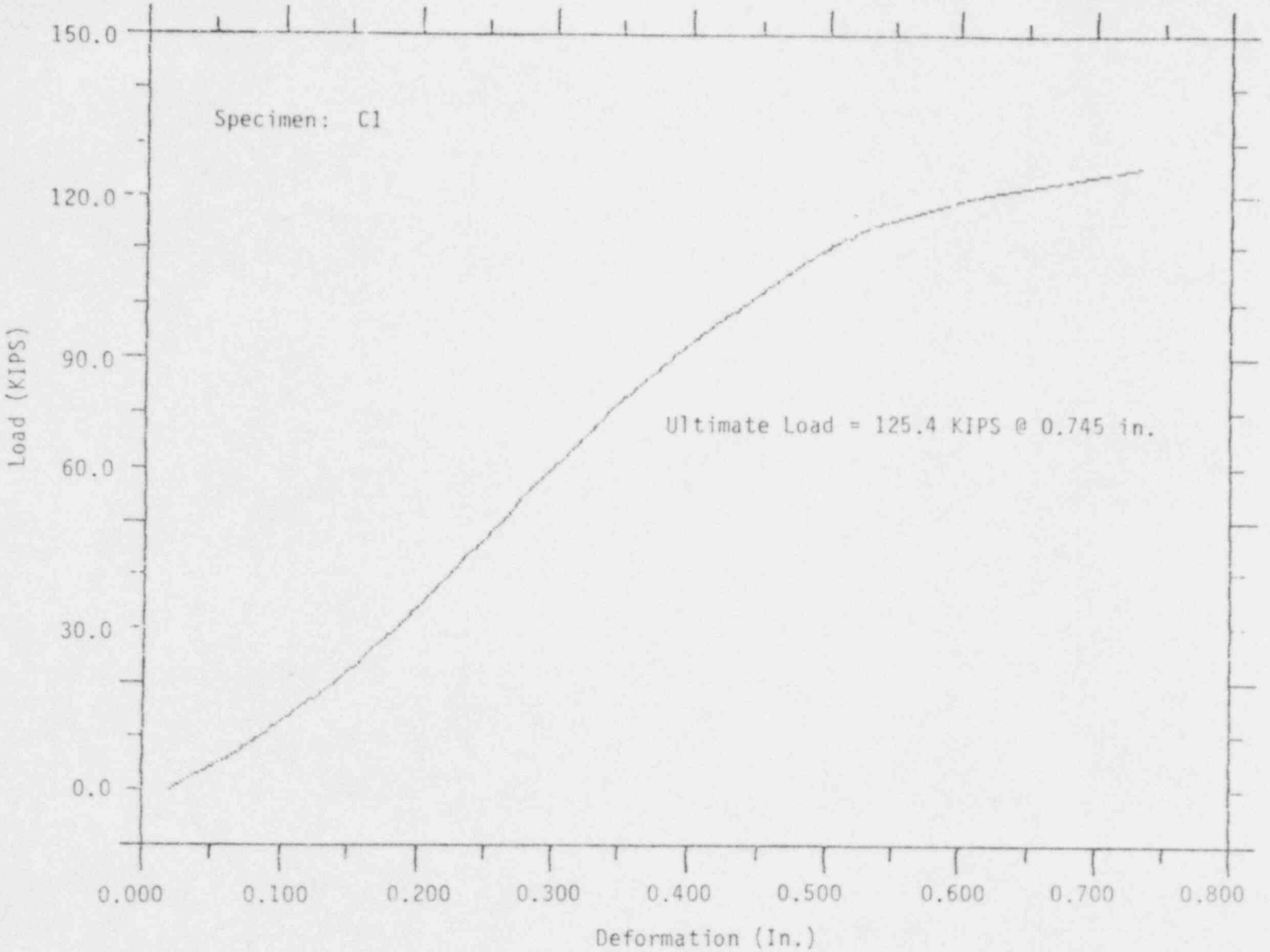

Figure 4-10 - Load Versus Dial Gage Extension.

Table 4-7

SUMMARY OF DISPLACEMENTS AND STRAINS

Specimen ID	Rod Max. Load (KIP)	Rod/Weld Displ. (In.)	Weld Height (In.)	Calc. Weld. Displ. (In.)	Theor. Rod Strain (1)	Overall Rod/Weld Strain (2)	Average Weld Strain (3)	
B1	55.7	0.000	0.4400	-0.0264	0.24E-02	0.000	-0.041	Gauge slipped
B3	63.2	0.166	0.4500	0.1380	0.27E-02	0.015	0.212	
B4	68.8	0.171	0.4900	0.1406	0.29E-02	0.015	0.220	
B5	61.6	0.159	0.4600	0.1315	0.26E-02	0.014	0.202	
B6	55.4	0.120	0.4400	0.0953	0.24E-02	0.011	0.147	
B7	47.3	0.100	0.3900	0.0800	0.20E-02	0.009	0.123	
B9	65.0	0.146	0.4400	0.1166	0.28E-02	0.013	0.179	
B10	62.2	0.168	0.4400	0.1405	0.26E-02	0.015	0.216	
B13	59.8	0.140	0.4700	0.1135	0.25E-02	0.013	0.175	
B14	67.2	0.173	0.4400	0.1432	0.29E-02	0.016	0.220	
C1	125.4	0.500	0.5400	0.4645	0.24E-02	0.032	0.929	
C2	151.0	0.372	0.6400	0.3338	0.28E-02	0.027	0.556	
C3	135.0	0.341	0.6300	0.3069	0.25E-02	0.024	0.511	
C4	142.5	0.331	0.6200	0.2950	0.27E-02	0.024	0.492	
C5	132.5	0.329	0.5900	0.2954	0.25E-02	0.023	0.537	
C6	143.0	0.336	0.6100	0.2997	0.27E-02	0.024	0.545	
C8	147.0	0.323	0.5900	0.2864	0.28E-02	0.023	0.521	
C9	125.0	0.422	0.5600	0.3890	0.24E-02	0.029	0.778	
C10	141.5	0.312	0.5900	0.2762	0.27E-02	0.022	0.460	
C12	137.5	0.318	0.5800	0.2839	0.26E-02	0.023	0.473	
D1	240.5	0.442	0.7300	0.4068	0.26E-02	0.030	0.581	
D2	241.3	0.634	0.7300	0.5987	0.26E-02	0.044	0.855	Gauge slipped
D3	222.5	0.366	0.7200	0.3339	0.24E-02	0.026	0.514	
D4	222.8	0.553	0.7500	0.5204	0.24E-02	0.038	0.743	
D5	247.3	0.415	0.7400	0.3788	0.26E-02	0.029	0.541	
D7	237.5	0.391	0.7000	0.3569	0.25E-02	0.027	0.510	
D8	226.3	0.389	0.7200	0.3565	0.24E-02	0.027	0.509	
D10	226.5	0.381	0.6900	0.3490	0.24E-02	0.027	0.499	
D11	255.0	0.553	0.7500	0.5170	0.27E-02	0.039	0.739	
D12	237.8	0.437	0.7300	0.4021	0.25E-02	0.030	0.619	

1. Theor Rod Strain = Stress/Modulus of Elasticity
2. Overall Rod/Weld Strain = Total Deflection/Gauge Length
3. Average Weld Strain = (Total Displacement-Rod Displacement)/Weld Length

FRACTOGRAPHIC ANALYSIS

In addition to the metallurgical analysis to identify the metallurgical structure of the welds, two specimens that had been tested were examined to clarify the nature of the failure.

The two specimens examined were C8, which did not exhibit a pre-existing crack, and C3, which contained a pre-existing (i.e., prior to testing) crack near the root of the weld.

Fracture Surface Appearance of Specimen C8

Figure 4-11 shows the failed weld after testing from Specimen C8. This view is looking at the cut end of the one and one-half inch diameter rod and the fracture surface. A close view of the fracture surface in the weld is shown in Figure 4-12. The origin is at the center of this picture. This region is shown at a higher magnification (13.5X) in Figure 4-13. Here again, the origin region is shown clearly and it appears to indicate intergranular initiation below the weld surface with the fracture propagating towards the surface and the root of the weld.

To get a better indication of the fracture morphology, the specimen was cut and mounted for the scanning electron microscope (SEM). A series of pictures depicting the region of the origin and the features each side of it are shown in Figures 4-14 through 4-17. It is clear from Figures 4-14 and 4-15 that the origin region is intergranular fracture, whereas, each side of the dimple rupture morphology is apparent as the crack progresses into the weld and to the surface and to the root of the weld (Figures 4-16 and 4-17).

Fracture Surface Appearance of Specimen C3

A detailed examination of Specimen C3 was also performed to clarify the nature of the pre-existing cracks. A view of the fracture surface with the crack shown as the darker region in the lower part of the picture is shown in Figure 4-18.

Figure 4-11 - Fracture Surface of Specimen C8.

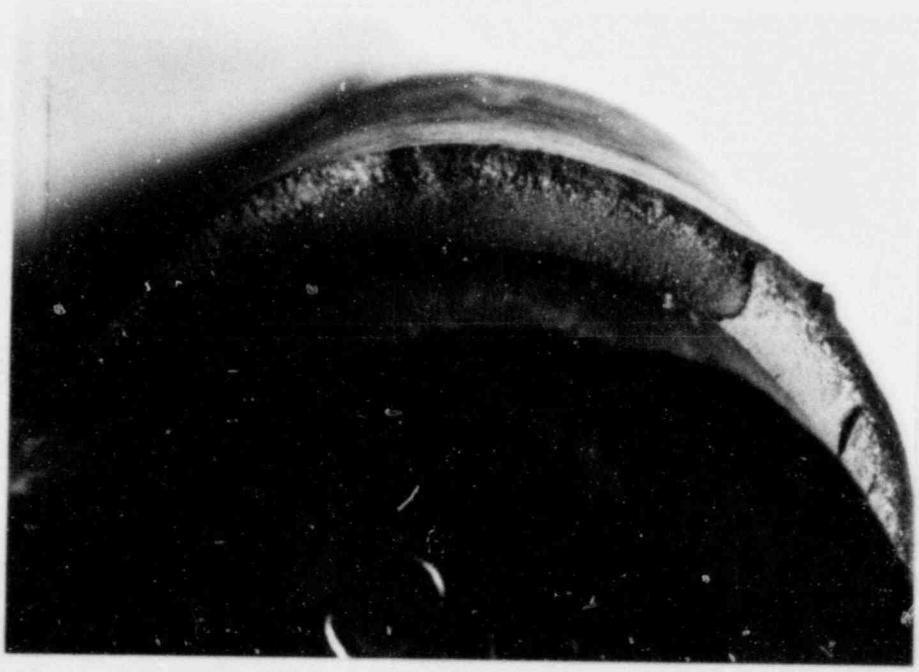

MAG:3.7X

Figure 4-12 - Origin Region of Test Specimen C8.

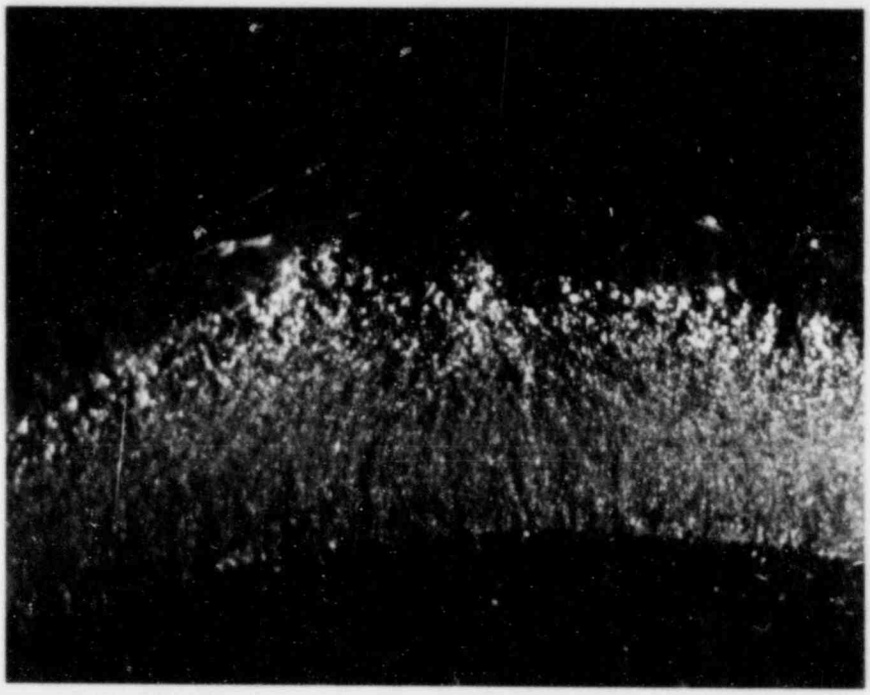

MAG:~13.5

Figure 4-13 - Fracture Surface Near Origin.

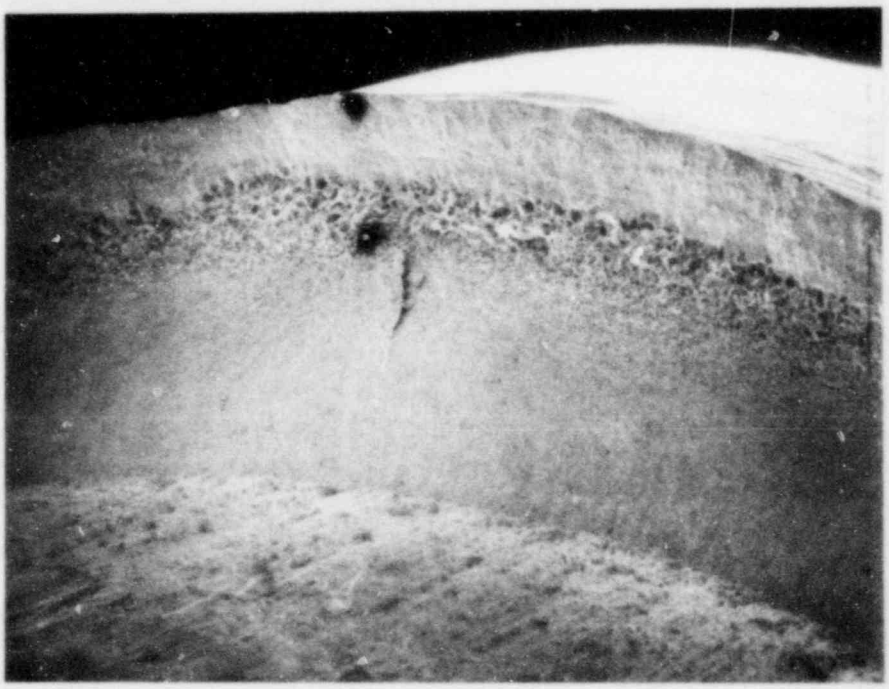

MAG:~12X

Figure 4-14 - SEM Photograph of Specimen C8 Fracture Surface.

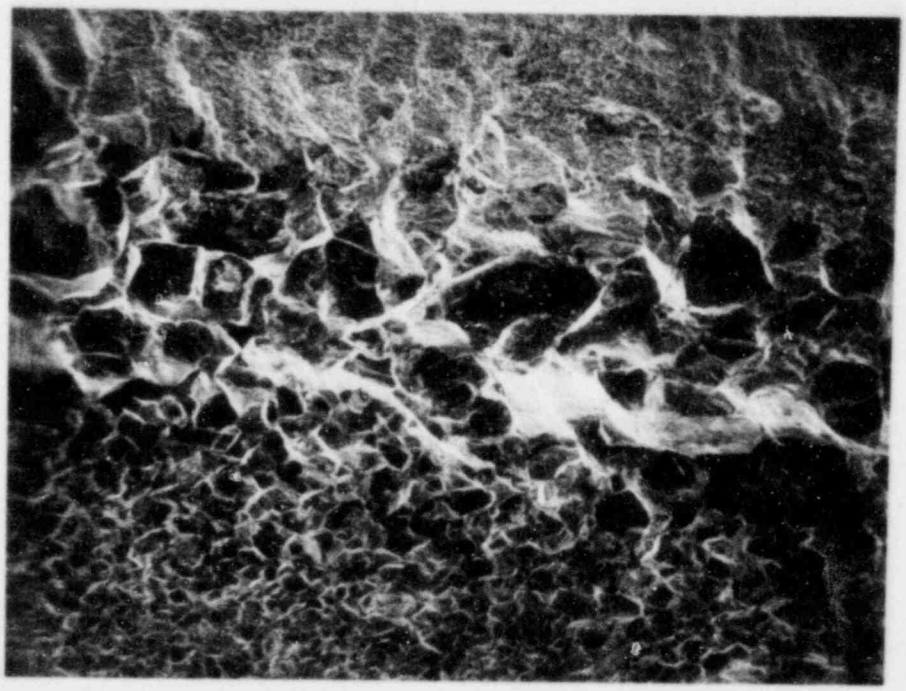

MAG:100X

Figure 4-15 - Intergranular Fracture on Fracture Surface of Specimen C8.

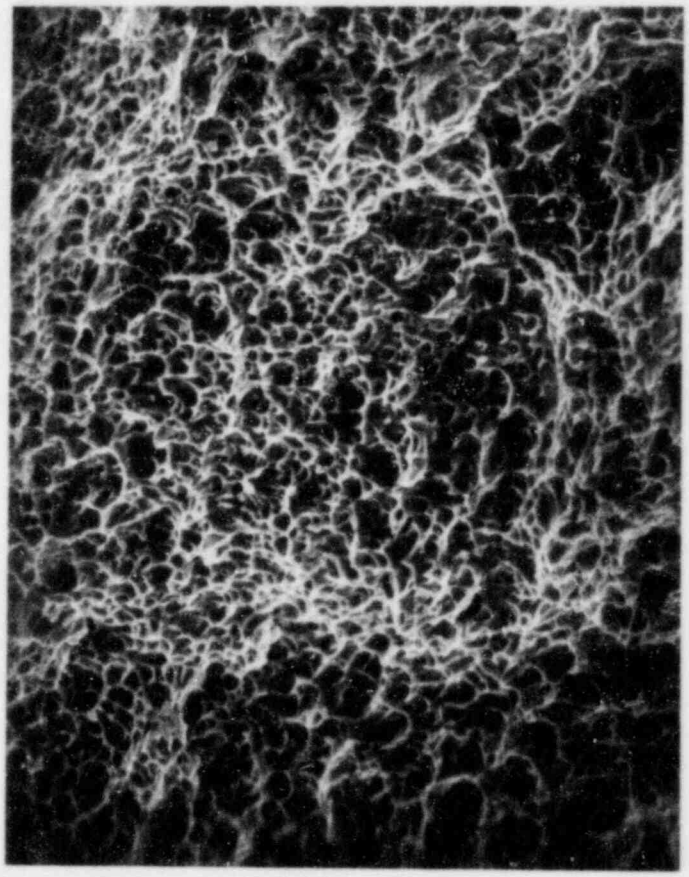

MAG:500X

Figure 4-16 - Region of Dimpled Rupture Towards OD From Intergranular Region.

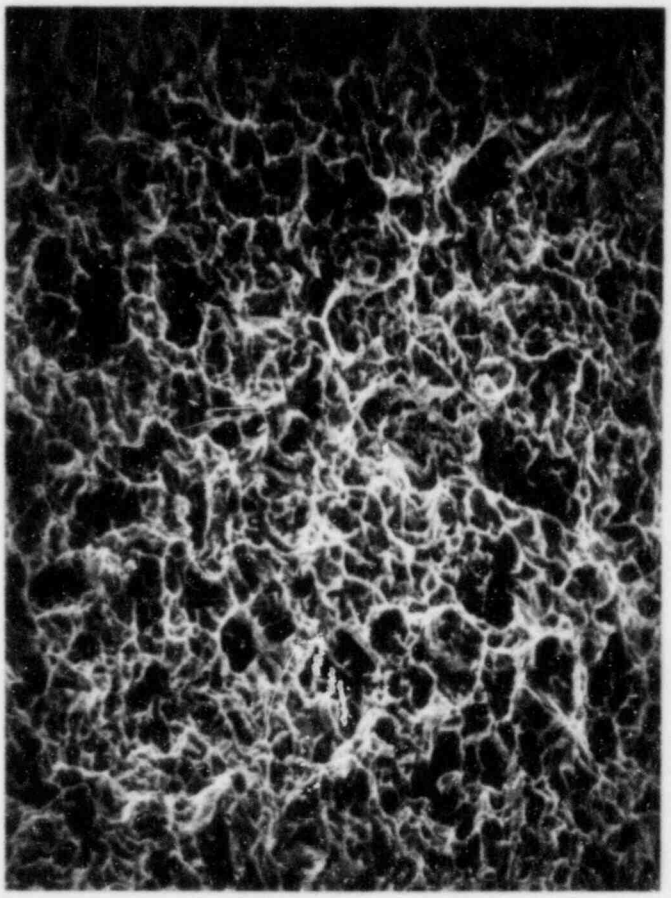

MAG:500X

Figure 4-17 - Region of Dimpled Rupture Towards ID From Intergranular Region.

MAG:~7X

Figure 4-18 - Fracture Surface of Specimen C3 Showing Pre-Existing Crack (Dark Region).

Again, an intergranular fracture morphology is present near the origin of this crack.

This specimen was cut and examined in the SEM to determine the fracture micromorphology.

Figures 4-19A and 4-19B show the intergranular nature of the crack although the surface is also covered with oxide. Outside this region, the fracture surface shows a dimple appearance typical of ductile failure (Figure 4-20).

Both fracture surfaces show that the origin region (for the fracture and the crack) are intergranular and the crack propagates by a ductile rupture mechanism outside this area. This indicates that the strength of this detail is controlled by the strength properties of the material through which the crack propagates.

In summary, the cracks appear to initiate in the hard HAZ of the A193-B7 rod and link back to the root of the weld.

FRACTURE ANALYSIS

Although all of the test specimens failed at loads greater than the specified ultimate capacity for A36 rods, a fracture analysis was performed to ensure that there was no potential for a low stress brittle fracture.

It was also noted from the fractographic analysis of the broken test specimens that the failures appeared to initiate below the weld metal surface near the throat of the weld and propagated through weld metal and HAZ in a ductile manner in the rod material. No rod failures were initiated at the weld toe on the rod even though undercut was apparent in some specimens.

To analyze the load capacity of A36 or A193-B7 rods welded to A36 plate using a weld procedure for A36 materials and E7018 welding electrodes, considering weldments containing defects or pre-existing cracks, various potential failure

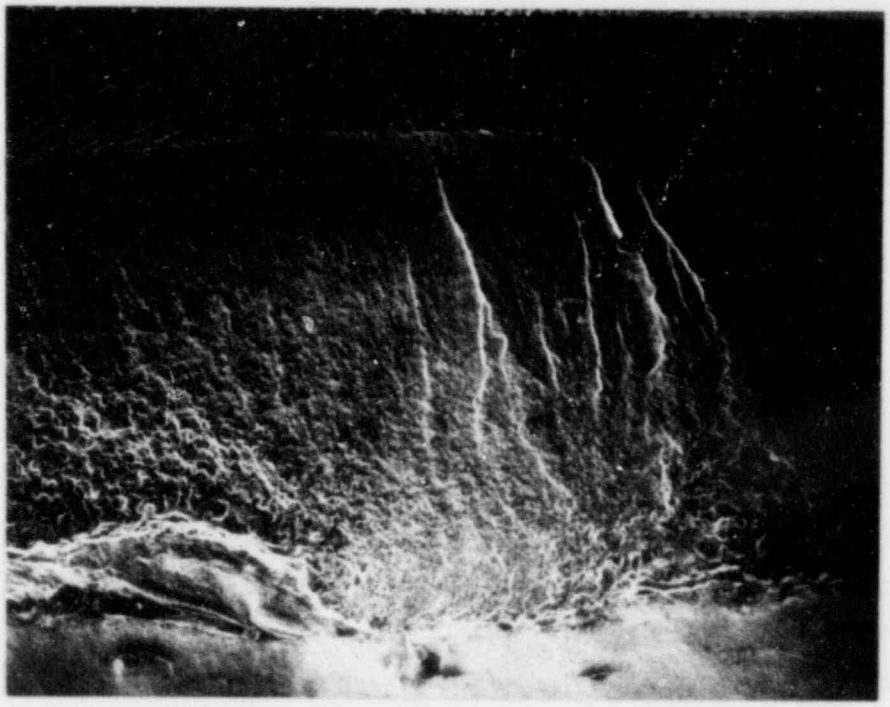

MAG:20X

Figure 4-19A - SEM Fractograph of Specimen C3 in Region of Discoloration.

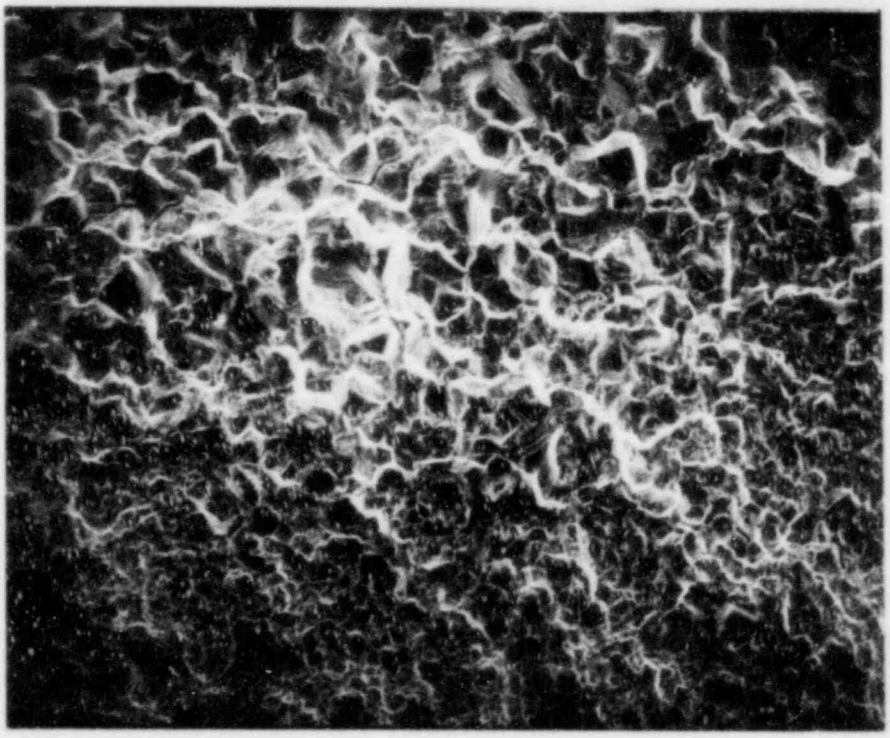

MAG:100X

Figure 4-19B - Region of Integranularity in Specimen C3.

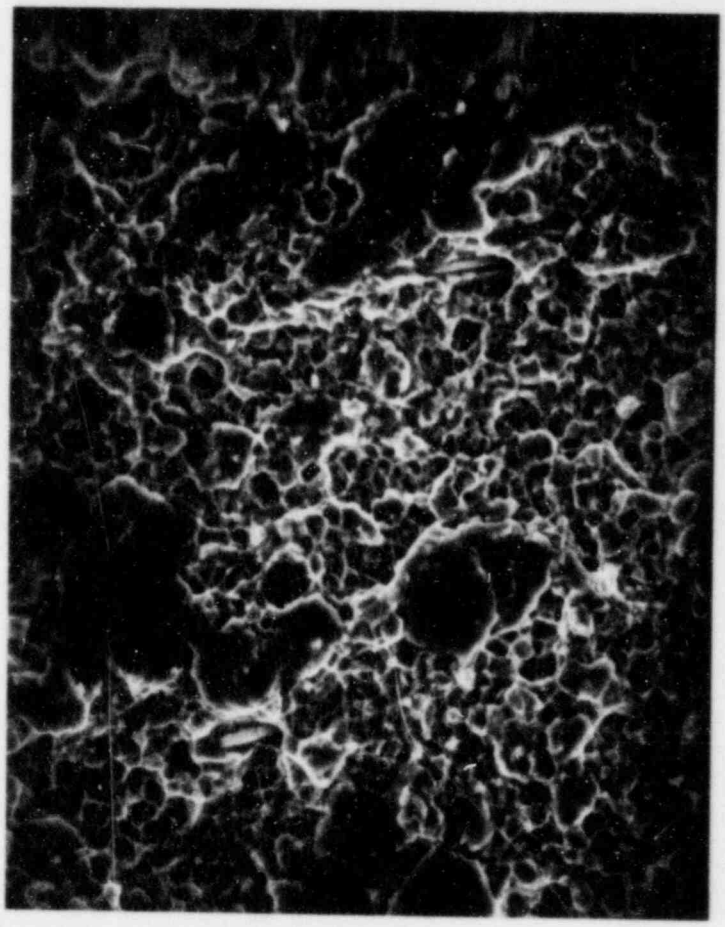

MAG:500X

Figure 4-20 - Oxidized Region of Dimple Rupture Towards OD From Region of Intergranular Fracture in Figure 4-19B.

mechanisms and flaw locations were postulated. The following models were proposed:

Type IA - Fracture initiation from toe cracks located around the anchor rods

Type IB - Plastic collapse in the net section near toe cracks located around the anchor rods

Type IIA - Fracture initiation from root cracks located parallel to the circumference of the anchor rods

Type IIB - Shear failure of the weld metal or the rod subcritical HAZ

Type IIIA - Fracture initiation from root crack parallel to the A36 plate

Type IIIB - Plastic collapse of the weld metal with flaws located in the plane of the minimum weld throat

Figure 4-21 is a schematic showing the location of the postulated discontinuities. Examinations of the metallurgical sections and the fracture surfaces of the test specimens indicate that only Type II discontinuities were present in these weldments (2). These discontinuities were cracks extending approximately one-quarter inch from the weld root in a plane parallel to the axis of the anchor rod. They are located in the A193-B7 coarse grained HAZ and have an intergranular fracture and ductile morphology. Although the presence of these cracks on the fracture plane suggests that they may have participated in the failure of the test specimens, there are also test specimens in which no pre-existing defects were observed on the fracture surface. Since the load capacities of the test specimens with pre-existing cracks on the fracture surface were similar to the capacities of those with no apparent defects, the reduction in load capacity due to pre-existing defects of this type with a depth of one-quarter inch or less is minimal (2).

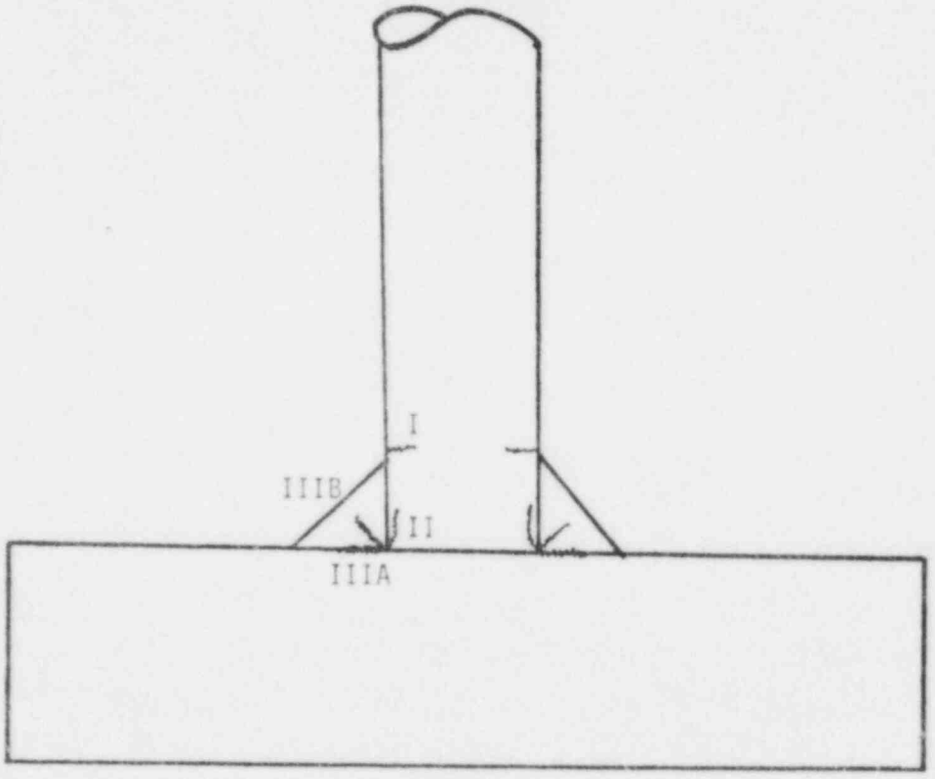

Figure 4-21 - Schematic of Possible Flaws Which May Result in a Reduction in Load Capacity of the Embed.

Failure of the weldments in the presence of Type II cracks could occur by either plastic collapse or brittle fracture initiation. Both of these failure mechanisms have been addressed. Since it is clear from the fractography that a ductile failure mode predominates in the tests, the analysis methods developed first are based on limit load. To confirm that there is no potential for low stress brittle fracture, fracture mechanics analyses have also been performed.

PLASTIC COLLAPSE

Plastic collapse for the weld configurations tested will occur when the net section shear stress, σ_{net}, is greater than or equal to the shear strength, τ_{crit}, of the uncracked ligament. The critical load, P_c, can thus be obtained by multiplying the critical shear stress, τ_c, by the net area in the presence of a crack.

$$P_c = \tau_c \times Area_{net} \qquad (4\text{-}1)$$

The critical shear strength of E7018 weld metal was calculated as the value of the tensile flow stress, σ_f, divided by $\sqrt{3}$, as is considered appropriate based on the Von Mises yield criteria. For limit load analyses of steel structures, it is common to use the average of the yield and ultimate strengths for the flow stress. This results in a value of critical shear stress of

$$\tau_c = \frac{\frac{60\ ksi + 70\ ksi}{2}}{\sqrt{3}} = 38\ ksi \qquad (4\text{-}2)$$

where, 60 ksi and 70 ksi are the specified minimum yield and ultimate strength of the weld metal, respectively.

The net section area of any particular rod was calculated by the following equation:

$$\text{Area}_{net} = \pi \times \text{Nominal Rod Diameter} \times (\text{Weld Leg Length} - \text{Crack Depth}) \quad (4\text{-}3)$$

Figure 4-22 shows the results of this analysis corresponding to collapse of E7018 weld metal. This analysis is based on a crack in the weld throat plane, all the way around the weld.

The cracks observed on the test specimens and the subsequent crack path were in part located in the A193-B7 material (2), thus, root cracks would result in an increase in the net section shear stresses in the A193-B7 HAZ more than in the E7018 weld metal. The plastic collapse analysis was, thus, performed a second time using the strength properties associated with a A193-B7 material tempered at 1290°F. This should provide the strength value for the softest HAZ region (i.e., the subcritical HAZ). Figure 4-23 shows the hardness of A193-B7 material as a function of tempering temperature. For a 1290°F (about 700°C) temper, the hardness is expected to be HRC 24.5. Using a standard table (see ASTM A370), this hardness value correlates to an ultimate tensile strength value of 118 ksi. Figure 4-24 shows ultimate tensile and yield strength values for A193-B7 tempered at slightly lower temperatures. The ratio of the yield strength to the ultimate tensile strength is approximately 0.9 for these data. Using this relationship, the yield strength for a 1290°F temper is estimated at 106 ksi. Using these values, an estimated shear strength is given as:

$$\frac{\frac{118 \text{ ksi} + 106 \text{ ksi}}{2}}{\sqrt{3}} = 64.7 \text{ ksi} \quad (4\text{-}4)$$

This value was used to generate another series of load capacity versus crack depth to weld leg length ratios and is included in Figure 4-25. As is shown, the calculated load capacities of the embeds with axisymmetric weld root

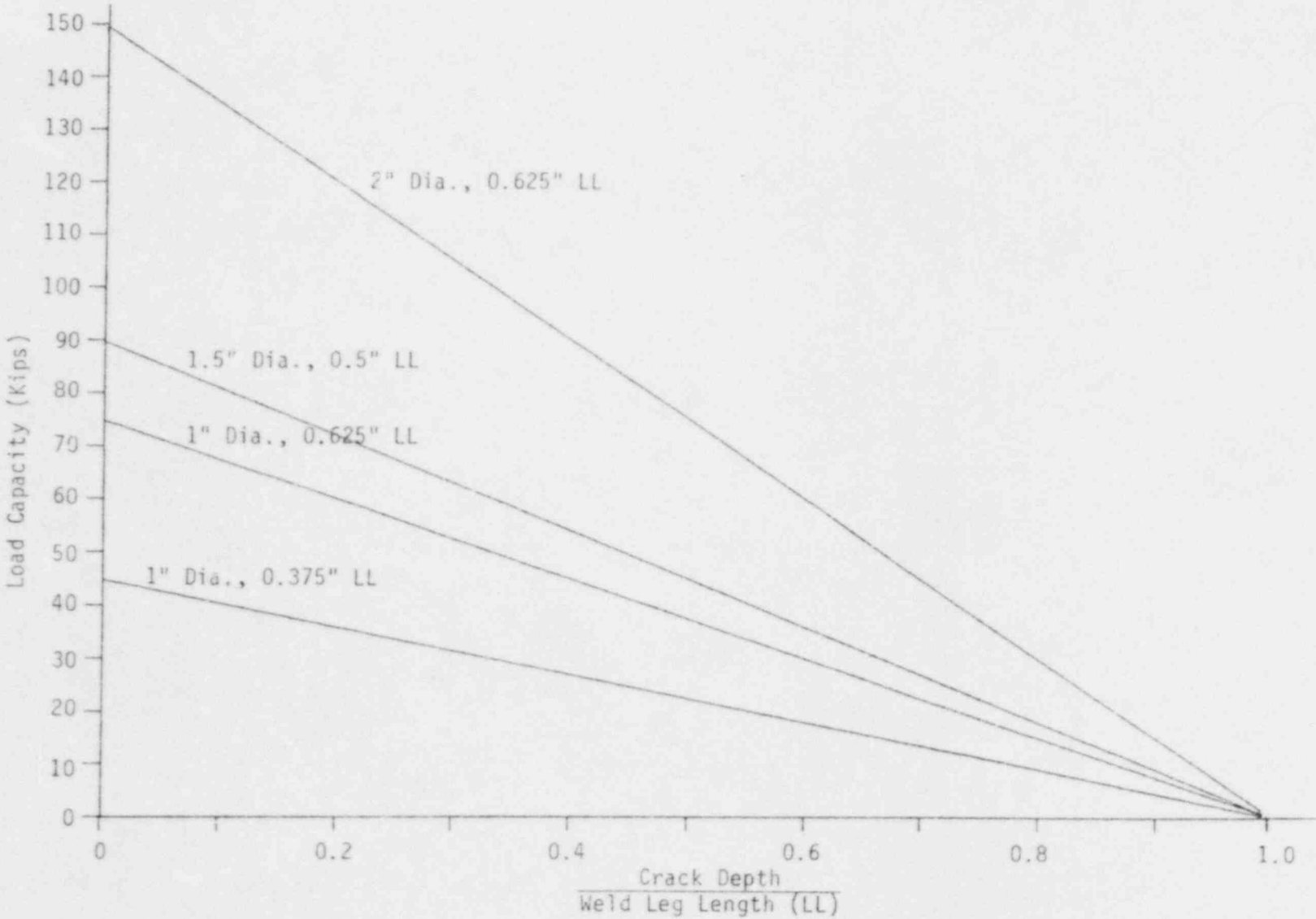

Figure 4-22 - Load Capacity Versus Crack Depth to Weld Leg Length Ratio For Plastic Collapse of E7018 Weld Metal (See Type II Cracks in Figure 4-21).

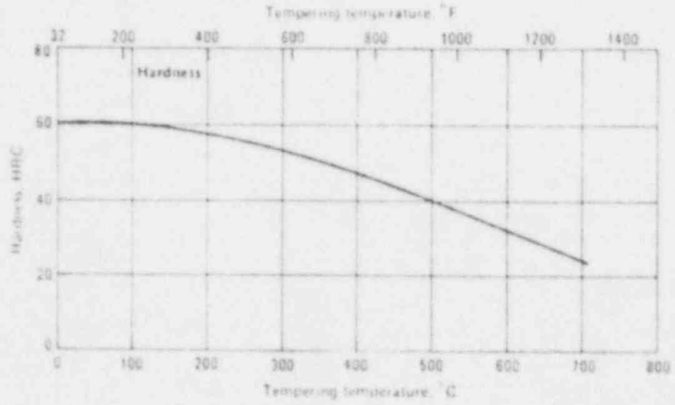

Figure 4-23 - Hardness Versus Tempering Temperature For A193-B7 Material (1).

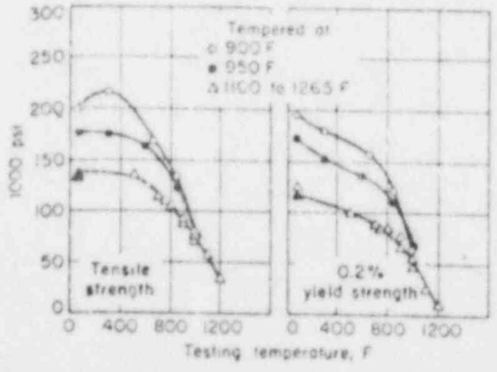

Figure 4-24 - Yield and Ultimate Tensile Strength Values For A193-B7 in Various Conditions and at Various Temperatures (1).

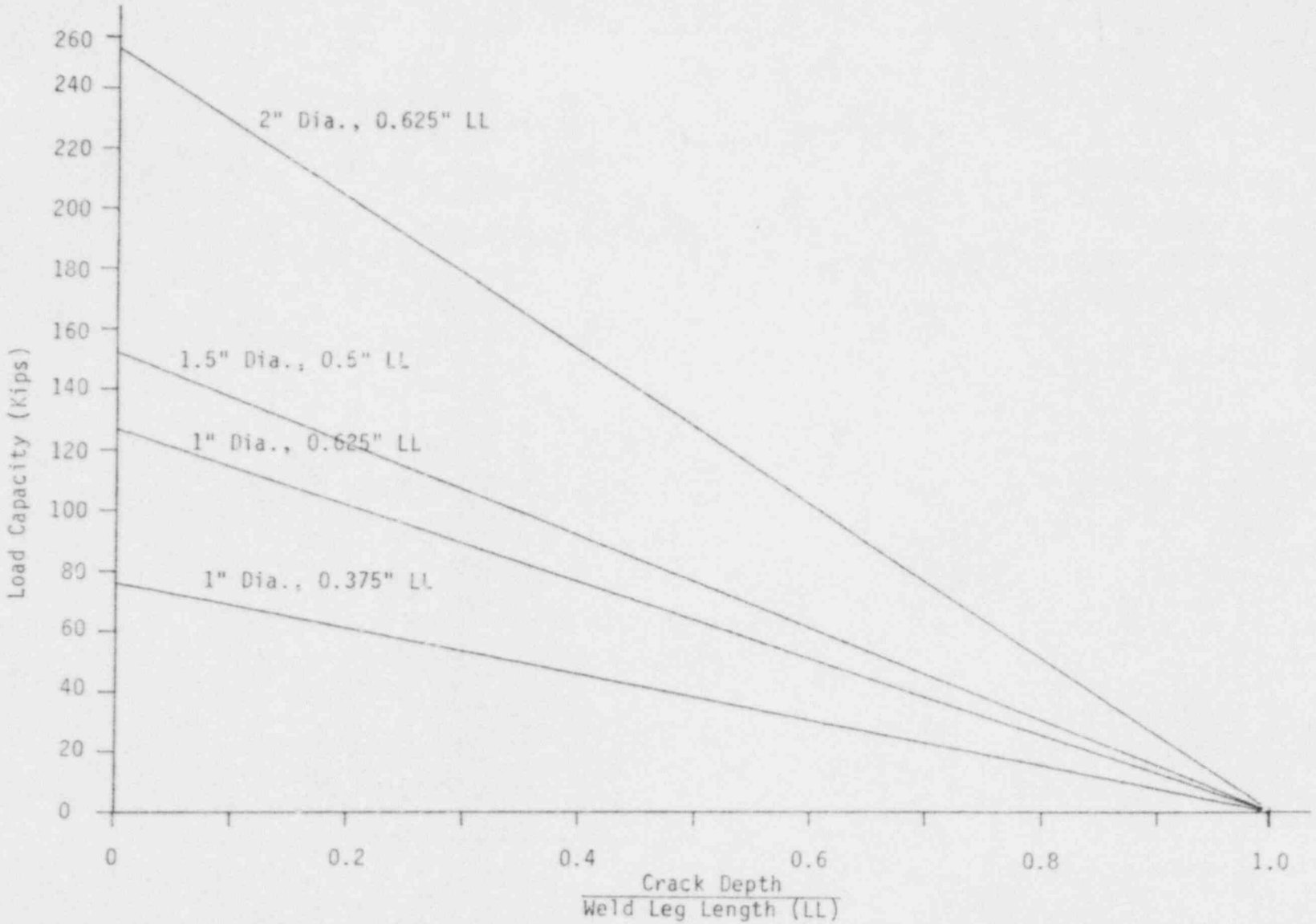

Figure 4-25 - Load Capacity Versus Crack Depth to Weld Leg Length For Plastic Collapse of A193-B7 Subcritical HAZ (See Type II Cracks in Figure 4-21).

cracks located within the A193-B7 HAZ are higher than the corresponding load capacity based on the weld metal properties for the same flaw size. With larger flaws present in this region than in the weld metal, this region could control.

The tested failure loads correspond to values analytically predicted for very small flaws by the foregoing model, which considers a crack all the way around the HAZ in the rod material. Therefore, it appears that the assumption of an axisymmetric continuous crack in the HAZ is too severe and an analysis considering short aspect ratio cracks would be more realistic. The model as postulated, however, does indicate that there is very little influence of the cracks in the HAZ on the measured failure loads.

As long as the cracks located in the weld HAZ do not appreciably increase the stresses in the weld metal, then significant cracks can reside in the A193-B7 HAZ without a loss in load capacity since even without any defects in the weld metal, the weld metal will be stressed above its critical shear stress prior to the net section stress in the HAZ becoming critical. This means that failure through the weld metal is likely in the tests since the limiting strength condition is the weld metal. This is, in fact, what occurred in the tests. Even with cracks present, ductile failure of the weld occurred.

FRACTURE MECHANICS ANALYSIS

Root Cracks

As a further check on the effect of the A193-B7 HAZ cracks, a linear elastic fracture mechanics analysis was performed to model these cracks. The cracks were modeled as edge cracks loaded by inplane shear stress. For this case, the Mode II stress intensity factor, K_{II}, is given (4):

$$K_{II} = \tau\sqrt{\pi a}\, F_{II} \qquad (4\text{-}5)$$

Where,

τ = Shear stress in the crack plane

a = Crack length

b = Thickness

F_{II} = Mode II stress intensity correction factor = f (flaw and specimen geometry)

$$= \left[1.122 - 0.561\left(\frac{a}{b}\right) + 0.085\left(\frac{a}{b}\right)^2 + 0.180\left(\frac{a}{b}\right)^3\right]\sqrt{1 - a/b}$$

Fracture initiation will occur when:

$$K_{IIC} < K_{II} \qquad (4\text{-}6)$$

However, for this particular detail and materials, no K_{IIC} data are available. In the fracture testing of steels, $K_{IC} < K_{IIC}$, and hence, K_{IC} values (the critical Mode I stress intensity factor) were used.

A critical stress intensity factor for the A193-B7 HAZ was estimated from Refs. (5) and (6). A value of 30 ksi$\sqrt{\text{in}}$ was used, which represents a lower bound of the reported values in Refs. (5) and (6). Figures 4-26 through 4-29 show the results of this analysis corresponding to fracture initiation in A193-B7 coarse grained HAZ. Again, it is found that failure would be expected to occur by shear failure in the weld, even if pre-existing defects are present in the A193-B7 coarse grain HAZ.

Since the strength properties used in these analysis were not based on the actual shear strength and fracture toughness levels of the A193-B7 HAZ and E7018 weld materials but rather were based on lower bound material properties, the calculated load capacities are less than the capacities actually measured

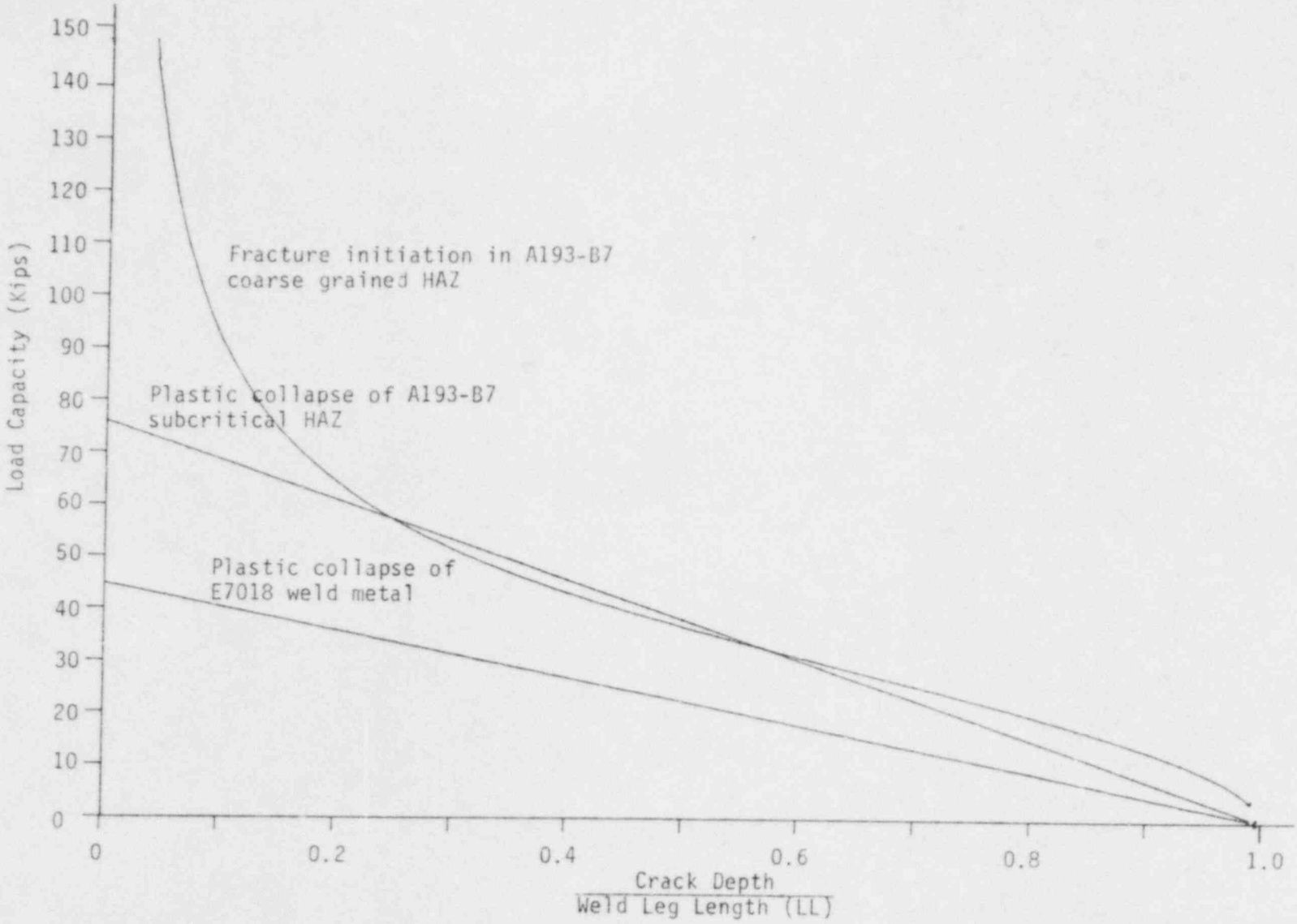

Figure 4-26 - Load Capacity Versus Crack Depth to Weld Leg Length Ratio For Type II Cracks (1" Diameter Rods With 3/8" Fillet Weld (0.375" LL)).

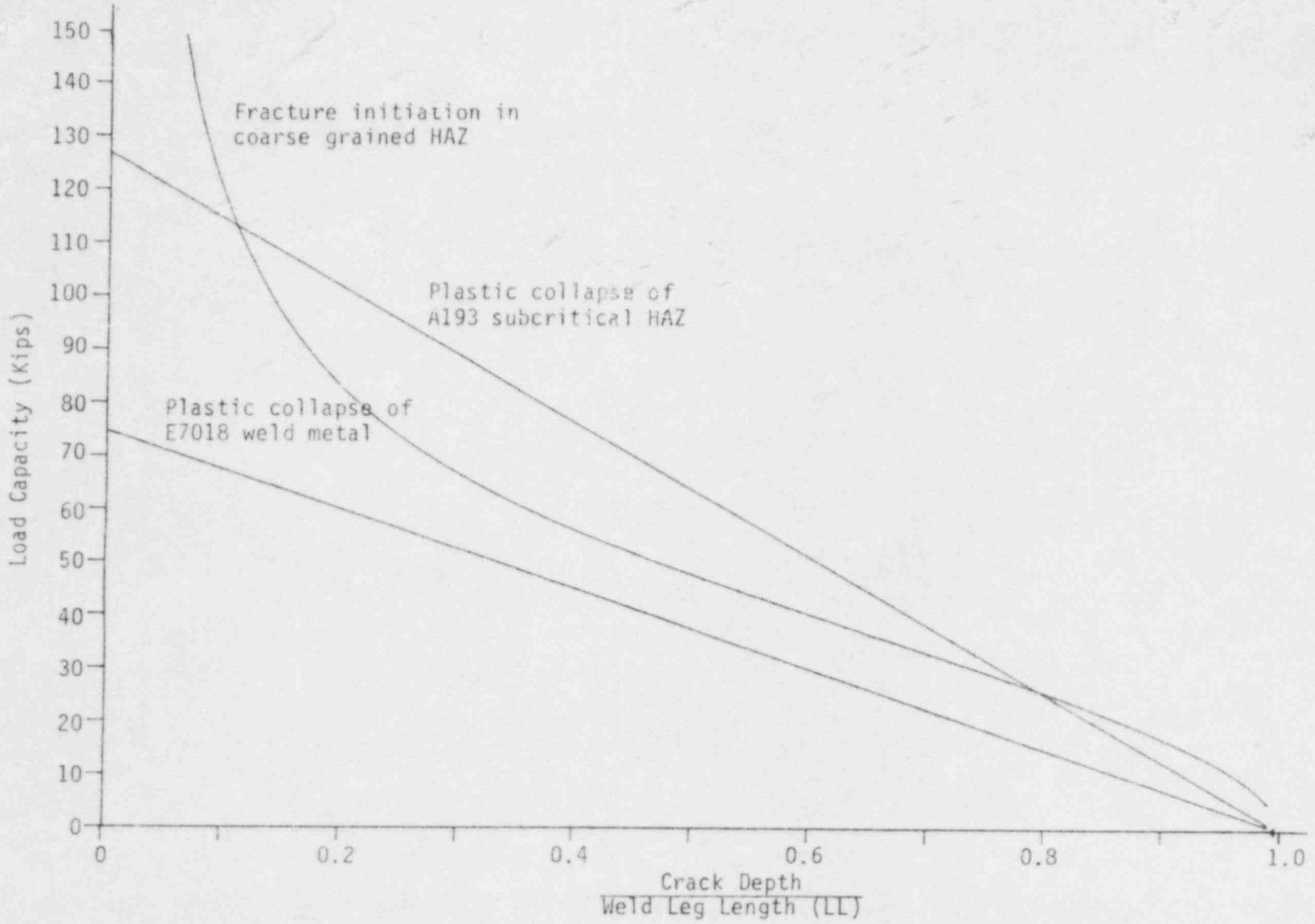

Figure 4-27 - Load Capacity Versus Crack Depth to Weld Leg Length Ratio For Type II Cracks (1" Diameter Rods With 5/8" Fillet Weld (0.625 LL)).

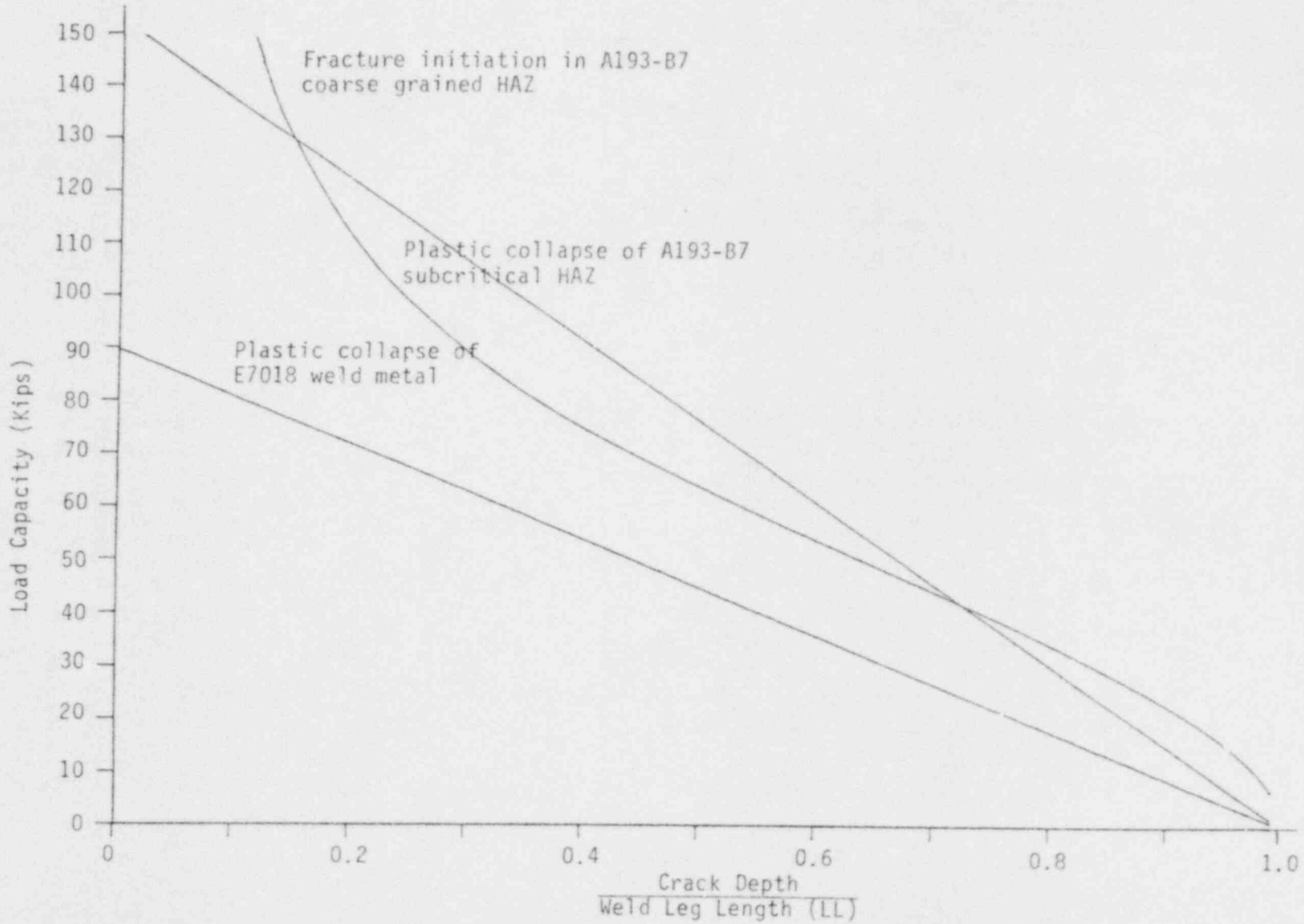

Figure 4-28 - Load Capacity Versus Crack Depth to Weld Leg Length Ratio For Type II Cracks (1-1/2" Diameter Rods With 1/2" Fillet Weld (0.5" LL)).

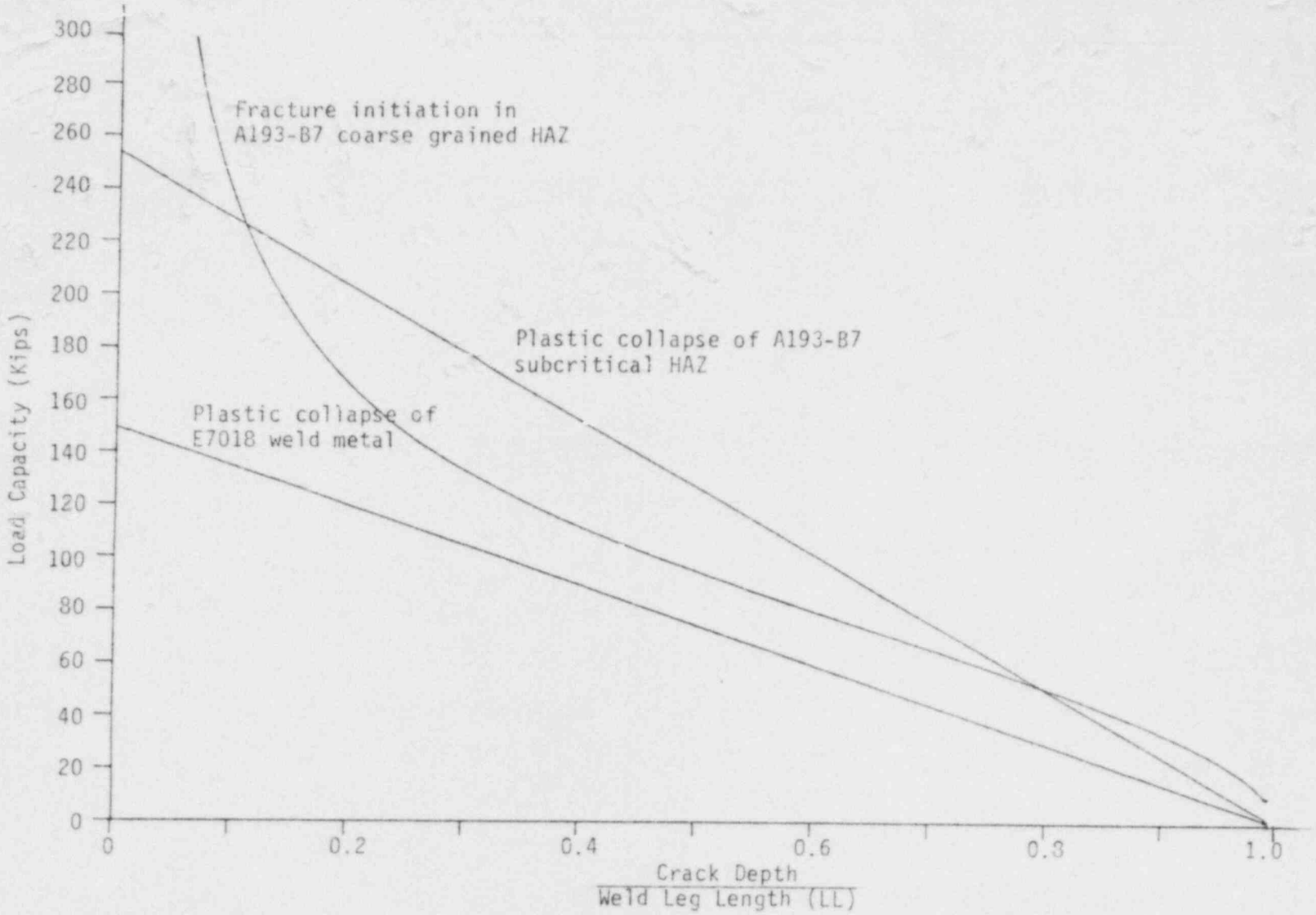

Figure 4-29 - Load Capacity Versus Crack Depth to Weld Leg Length Ratio For Type II Cracks (2" Diameter Rods With 5/8" Fillet Welds (0.625" LL)).

on these embeds. This simply shows the conservatism of the engineering models used in these plastic collapse and fracture mechanics models and that pre-existing cracks could be present in the A193-B7 HAZ near the weld root with no associated loss in load capacity.

Summary

The result of the analyses indicate that the plastic collapse mechanism controls for realistic flaw sizes. This substantiates both the test results and the ductile fracture morphology observed in the broken specimens. Composite curves for the three specimen sizes are shown in Figures 4-26 through 4-29.

Section 5
SIGNIFICANCE OF THE RESULTS

INTRODUCTION

It is clear from the foregoing discussion that in the A193 rod weldments under consideration there is no potential for low stress brittle fracture and that the failure is controlled by limit load of the weld and HAZ. The tested failure loads for the A193 rod weldments indicate no degradation with respect to the required load capacity dictated by the original design based on A36 rod weldments. For the one and one-half inch and the two inch diameter rods, the failure loads represented by the average test values (138 K and 235 K) as well as the statistically projected lower bound values (117 K and 209 K) are distinctly higher than the specified ultimate load capacity of 102 K and 182 K for A36 rods of one and one-half inch diameter and two inch diameter, respectively. For the one inch diameter rods, the failure load average test value (60.6 K) is higher than the ultimate load capacity, and the statistically projected lower bound (45.3K) is equal to the ultimate load capacity of 45.6 K for one inch diameter A36 rods. In this Section, the implications of the established ultimate load capacities on the design margins is discussed.

DESIGN BASIS

The allowable design load for anchor rods welded to embedded plates is determined from the allowable stresses prescribed by the AISC specification (7) multiplied by the corresponding cross-sectional areas of fillet weld or rod, whichever results in the lower design load.

The allowable load for fillet welds is specified as follows:

$$P_w = (0.3 \times \sigma_u \left(\frac{0.707}{16}\right) Aw \qquad (5\text{-}1)$$

where,

A_w = Area of the weld

= ℓ_w x (number of sixteenths of fillet weld size)

ℓ_w = Length of fillet weld = πD

D = Diameter of rod

σ_u = Ultimate tensile strength of weld metal (= 70 ksi for E7018 deposits)

0.707 = Sin 45°, applicable for effective throat of equal-legged fillet welds

Hence,

$$P_w = 0.928\ A_w \qquad (5\text{-}2)$$

This allowable load corresponds to a factor of safety (FS) with respect to the ultimate strength of the weld metal as follows:

$$FS = \frac{1}{0.3} = 3.3 \qquad (5\text{-}3)$$

The allowable load for rods in tension (P_t) is specified as follows:

$$P_t = 0.6\ F_y\ A_y \qquad (5\text{-}4)$$

where,

A_y = Nominal area of rod

F_y = Yield strength of rod metal (= 36 ksi for A36 rods)

Hence,

$$P_t = 22\ A \tag{5-5}$$

This allowable load corresponds to FS with respect to the yield strength and the ultimate strength of the rod as follows:

$$FS_y = \frac{1}{0.6} = 1.67, \text{ and } FS_U = \frac{58}{22} = 2.6 \tag{5-6}$$

It is noted that for rods in shear the allowable load is lower and does not govern for the comparison to fillet weld allowable loads which are specified as the same for tension and shear.

Thus, the FS for fillet welds is higher than that prescribed for structural steel, which reflects the variability of strength anticipated in production welding. The strength is sensitive to the individual workmanship, as represented by size and soundness of the fillet weld, and to the actual material strength of the deposited weld metal. These natural variations anticipated in weld strengths are evident in the test results, and accordingly, the low values, as well as the high values, are not to be construed as representative values to be used as the generalized strength for the production welds. For this reason, the test results have been considered as part of a natural distribution of values (i.e., log normal).

The FS of 3.3 is generically applied by the AISC Specification, as well as the AWS D1.1 Welding Code, to all fillet welds regardless of whether the welds are stressed in the longitudinal or the transverse direction. Also the generalized FS of 3.3 is preserved not withstanding that the test results of

Ref. (8), which are AISC confirmatory tests for the specification provisions, indicate minimum FS ranging from 2.67 for longitudinal to 4.06 for transverse fillet welds.

In view of the foregoing considerations, it is recognized that in order to address the adequacy of the tested ultimate loads of fillet weld with respect to the design criteria, it is necessary to compare the ultimate loads with the governing allowable design loads. The objective is to demonstrate that the achieved FS are consistent with the nominal FS of 3.3 and that the FS variations from individual tests are within acceptable bounds, rather than solely demonstrating that the tested ultimate loads are higher than the rod ultimate load. The corresponding comparison is presented in Table 5-1.

The tabulated results indicate that the required ultimate capacity to obtain the nominal FS of 3.3 is satisfied by all of the test results except the three lowest test value for one inch diameter rod. These cases afford FS = 2.7, 3.2, and 3.2, and are acceptable with respect to the lower bound of 2.67 for FS from individual test results as reported in Ref. (8) and is consistent with the variations in strength that are anticipated for fillet welds as described therein. The 90%/95% statistical projection for the lower bound of available load capacity results in a FS = 2.6. For similar reasons, pertaining to the natural variability expected in weld strengths, this is considered to be acceptable as a lower bound evaluation of the FS.

In summary, the statistically projected lower bound (45.3 K) for the available ultimate load capacity derived from tests satisfies the specified ultimate load for A36 rods, the tested ultimate capacity average values for each rod size satisfy the required factor of safety (3.5, 3.9 and 4.0 > 3.3), and all of the 30 test results have load capacities higher than the A36 rod ultimate load and afford factors of safety higher than the nominal FS of 3.3.

A comparison of the FS for each of the tested series is shown in Table 5-1.

Table 5-1

FACTORS OF SAFETY DETERMINED FROM TEST LOADS

	1" ϕ	1½" ϕ	2" ϕ
Design Allowable Load:			
A36 rod	17.3	38.8	69.1
E7018 weld (fillet size)	17.5 (3/8)	34.9 (1/2)	58.2 (5/8)
$P_{allowable}$ (governed by)	17.3 (rod)	34.9 (weld)	58.2 (weld)
Required Ult. Load to Develop P_a with FS = 3.3	57.1	115	192
Ultimate load of A36 rod	45.6	102	182
Tested Ultimate Load Capacities and Corresponding Factor of Safety (FS) with Respect to Allowable Load			
P_{mean} (FS)	60.6 (3.5)	138 (3.9)	235 (4.0)
$P_{test\ lowest}$ (FS)	47.3 (2.7)	125 (3.6)	222 (3.8)
$P_{90/95}$ (FS)	45.3 (2.6)	117 (3.4)	209 (3.6)

DYNAMIC LOADING CONSIDERATIONS

As noted earlier, the embedded plates with welded anchor rods perform a variety of functions including the support of pipe whip restraints. Loading rates under pipe whip events from a double ended pipe break are usually rapid, and design basis force/time functions are used to define the applied loads. However, the energy absorbing characteristics incorporated into the design of all restraint structures, produce rates of loading transmitted to the anchor rods that are substantially lower than the postulated forcing function for the applied loads. As outlined earlier, all tests were performed using slow (static) loading conforming to ASTM A370. The question of "what effect will impact loads have?" needs to be addressed.

As the loading rate on a steel structure is increased, the properties of the materials may change. In general, as the rate of loading increases, the yield stress increases and the toughness decreases. Therefore, under dynamic loading, the toughness may decrease. This effect is most marked in low strength structural steel and becomes less pronounced with higher strength steels.

Detailed analyses have been performed to establish loading rates for different types of structures (9). These have been compared to the loading rates that can be expected in impact (or dynamic) fracture tests. Loading rates are generally expressed as stress intensity factor rates or $\dot{K}$ in units of $ksi\sqrt{in}/sec$. Fracture test samples experience much higher loading rates ($\dot{K} \sim 10^5$ $ksi\sqrt{in}/sec$) than structures, including bridges, under most types of loading. Drop forging presses and ships in collisions are two cases that will generate loading rates similar to those experienced in impact tests.

In the present case (i.e., anchor rods) that may see attenuated rapid loading from pipe whip events, the highest (bounding) loading rates may be calculated from the force/time functions used in the design analysis. This analysis has been done for the stainless U-bar type of pipe whip restraints, and peak values of $\dot{K}$ are less than those experienced in impact tests. This analysis was also performed for the energy absorbing material (EAM) type of pipe whip

restraints, and the force/time response determined from tests of EAM indicate loading rates with $\dot{K}$ values less than these experienced in impact tests.

In the fracture analysis, a lower bound value of 30 ksi$\sqrt{in}$ was used for the toughness of the A193 weld region. This is a worst case toughness and would not be expected to change with impact loading. In any event, the load capacity is controlled by limit load analyses, which under dynamic loading, imply increased strength properties.

Section 6
CONCLUSIONS AND RECOMMENDATIONS

The program of work described in this report was aimed at establishing the integrity of embedded plates that may contain A193-B7 anchor rods welded in place of A36 rods. The following conclusions were reached as a result of the welding and load capacity tests, analysis of metallurgy, and fracture predictions:

- For the A193-B7 material, which is readily hardenable by heat treatment (or welding), peak HAZ hardness values are similar irrespective of preheat levels, thickness, weld interpass temperatures, type of weld, and arc energy levels. In other words, the material is readily hardened under all welding conditions used in the test matrix.

- Peak hardness values measured in the A193-B7 HAZ were of the order of 750 HV10.

- The welding procedures selected resulted in hard martensitic HAZs in which some cracks occurred.

- The welding procedures used in the field fabrication of test specimens bounded the field welding parameters from the field welding procedures and are, therefore, representative welding conditions.

- All tests were in accordance with APTECH requirements. Displacement measurements were made for each test as a function of load.

- In spite of the fact that the potentially commingled A193 rods have been welded with a nonconforming welding procedure, there is no

degradation in load capacity. The tested ultimate capacity average value for each rod size satisfies the required factor of safety, and all of the test results exhibit load capacities higher than the A36 rod ultimate load.

- The fracture and limit load analysis indicated that there was little potential for brittle fracture with the observed flaw sizes. This was confirmed by the test results.

- In view of the above conclusions, it is proposed that the potential use of A193-B7 rods welded to A36 plate, using a welding procedure specified for A36 material, does not represent a degraded condition, and the embedded plates can be used "as is."

REFERENCES

1. American Society For Metals, Metals Handbook, 9th Edition, Vol. 1, "Properties and Selection: Irons and Steels" (1979).

2. Interoffice Memorandum, G. R. Schmidt to R. W. Stralton (Bechtel Materials and Quality Service Department), "Anchor Bolt Evaluation, South Texas Project," GRS-074-13 (June 27, 1984).

3. Interoffice Memorandum, G. R. Schmidt to R. W. Stralton (Bechtel Materials and Quality Service Department), "Anchor Bolt Evaluation, South Texas Project," GRS-094-03 (September 10, 1984).

4. Tada, H., Stress Intensity of Cracks Handbook, Del Research Corporation, St. Louis, Missouri (1973), Pp. 229.

5. Air Force Materials Laboratory, Damage Tolerant Design Handbook, MCIC-HB-01 (January 1975).

6. Steigerwald, E. A., "Plane Strain Fracture Toughness of High Strength Steel Materials," Engineering Fracture Mechanics, Vol. 1 (1969), Pp. 473-494.

7. American Institute of Steel Construction, Inc., Manual of Steel Construction, 7th Edition, New York, NY.

8. "Proposed Working Stresses For Fillet Welds in Building Construction," AISC Engineering Journal (January 1969).

9. IIW Commission, "Some Proposals For Dynamic Toughness Measurements," UK Briefing Group On Dynamic Testing, Welding Institute Conference (1978).

Appendix A
RECOMMENDATIONS FOR STATISTICALLY-BASED LOWER BOUNDS

INTRODUCTION

The strategy used to establish the load capacity of a single embed rod employed an analysis of tensile load data of exemplar materials and fabrication. The uncertainty in expected load capacity was conservatively assessed by the following assumptions:

- The welding parameters were purposely selected in the fabrication of the test samples to promote a worst case situation with regard to ductility in the weldment.

- The test results were evaluated by statistical analysis to establish a lower bound estimate of load capacity.

By adhering to the above conditions, a conservative estimate of load capacity will be established. The statistical treatment of the data provides the assurance that the population of embeds will have at least the established capacity level given a stated probability of occurrence and a stated level of confidence. The criteria for probability and confidence levels are developed in this Appendix.

STATISTICALLY-BASED BOUNDS

A statistically-based bound is more appealing than a simple lower bound treatment of data because it provides a rational basis for establishing a conservative limit to both present and future observations. In the statistical treatment of the test data, a minimum or one-sided tolerance limit for the population of embed welds was established based on standard statistical methods and suitable criteria. The load capacity where there is X% probability that past and future observations will fall at or above some minimum level with a confidence of Y% is expressed as

$$P\left\{P\left\{F \geq F_C\right\} > X\%\right\} = Y\% \qquad \text{(A-1)}$$

Where, $P\{\}$ is the symbolic representation for the probability statement, F is the load, and F_c is the load capacity. Equation (A-1) is a definition for load capacity in statistical terms. The values selected for X and Y are, therefore, the parameters that constitute the criteria in the determination of load capacity.

STATISTICAL CRITERIA

Although the criteria selected for use in statistical analysis can be arbitrary and usually dictated by the judgements of the analyst, an attempt was made to select probability and confidence levels that are both reasonable (not overly restrictive) and consistent with industry practice. In the computations of load capacity, a 90%/95% (X%/Y%) and a 95%/95% were both determined as part of a sensitivity study. It is recommended that the 90%/95% criteria be used on the basis of precedents established in the industry.

A probability level for occurrence was selected on the basis of the criterion used in NUREG-0577 (A-1) for determining a bound on toughness data for component support materials. The materials and applications of component supports are similar to those used in embedded plate systems. In support of this criterion are the design allowables established in MIL-HDBK-5 (A-2) for use in arriving at design values for aerospace structures and elements.

The A-basis and B-basis properties in MIL-HDBK-5 have ascribed to them a 99% and 90% probability level, respectively. The B-basis criterion establishes the material design values for components or elements where no single failures of that component or element will cause failure of the complete system to perform its function. It has been judged that this criterion is consistent with the application of embed systems. With regard to the level of confidence that is acceptable for bounding material properties, a 95% confidence level is used in both A-basis and B-basis allowables. Hence, in the analysis, a 95% confidence level is used for computing the tolerance limits.

SUMMARY

A statistical treatment of the test data will provide a rational basis for establishing a conservative estimate for load capacity.

It is recommended that a 90%/95% criterion be used in establishing the load capacity of an embed rod on the basis of industry practice.

REFERENCES

A-1 Snaider, R. P., et al., "Potential For Low Fracture Toughness and Lamellar Tearing on PWR Steam Generator and Reactor Coolant Pump Supports," U.S. Nuclear Regulatory Commission Report, NUREG-0577, Rev. 1 (Octobe 1983).

A-2 Moon, D. P., and W. S. Hyler, "Guidelines For the Presentation of Data," MIL-HDBK-5, AFML-TR-66-386.